Collisionally Inhomogeneous Bose-Einstein Condensates

Chang Wang
St Hugh's College
University of Oxford

A thesis submitted for the degree of
MSc. in Mathematical Modelling and Scientific Computing

September 2011

Acknowledgements

I would like to thank my supervisor Dr Mason Porter, for his helpful guidance and suggestions throughout this project.

I would like to thank Dr Kody J H Law at the University of Warwick for his explanations and clarifications in our discussions and correspondence. I would also like to thank him for permission to use his code for solving the stationary and time-dependent GP equation.

Abstract

This dissertation studies solitary waves in collisionally inhomogeneous Bose-Einstein condensates in a magnetic trap using a quasi-1D mean-field model. We introduce a model for Bose-Einstein condensate with spatially and temporally modulated nonlinearity. In terms of the spatially periodic nonlinear lattice, we study BECs in a lattice one of which minimum in a period either overlap with the minimum of magnetic trap (termed 'aligned') or is displaced by $\frac{\pi}{2}$ (termed 'misaligned'). In BECs in an aligned and misaligned lattice, both bright solitons and dark solitons are identified. Stability analysis using the BdG equations shows that bright solitons with this spatial modulation are always stable, whereas dark solitons can be either stable or unstable. A further investigation of how their stability depends on physical parameters reveals that the aligned and misaligned lattices introduce different behaviours. Unstable dark solitons can have both real eigenvalues and a quadruplet of four eigenvalues in an aligned lattice. In contrast, unstable dark solitons in BECs in a misaligned lattice can have only real eigenvalues. We also investigate the temporal evolution of both bright solitons and dark solitons in a dynamical nonlinear lattice. After studying the response of bright solitons and dark solitons to the turning on of a nonlinear lattice, we can expect a stable transition if the turning on is slow. If the lattice is abruptly turned on, instability occurs.

Contents

List of Figures

Chapter 1

Introduction

In this dissertation, we study the existence, stability, and dynamics of solitary waves in Bose-Einstein condensates with collisionally inhomogeneous nonlinearity.

A BEC is a gas of weakly interacting bosons (identical subatomic particles that obey Bose-Einstein statistics) trapped by external potential that condensate into the same quantum (ground) state when temperature is below a critical point $T_c = 3.31 n^{2/3} \hbar^2/(m k_B)$, where $\hbar$ is the reduced Planck constant, n is the particle density, m is the mass of the boson, and k_B is the Boltzmann constant. The critical temperature T_c is very close to absolute zero and is of the magnitude of several kelvins [5]. For instance, T_c is 3.13 kelvin for liquid ^{4}He at saturated vapour pressure [18]. Current techniques allow a few thousands to several million particles condensating in a BEC [4] and temperature as low as 100 picokelvin have been reached [3].

Since its prediction by Bose and Einstein from quantum statistics in the 1920s, BECs have been investigated actively and were created in laboratory for the first time in 1995. The experimental realisation was delayed due to extreme difficulty in creating ultra-low temperature required to condensate enough bosons into the same state. Since then, laboratory techniques of controlling and monitoring BEC has progressed greatly and now key properties of a BEC can be accurately adjusted experimentally [5]. As a result BEC offers a wide variety of phenomena for physicists and applied mathematicians.

A BEC is a many-body Hamiltonian system. Due to the dilute nature of most BECs, as typically, the mean spacing between bosons is ten times greater than the range of inter-atomic forces, the interaction can be simplified by a mean-field approximation to obtain the Gross-Pitaevskii (GP) equation [2]:

$$i\hbar \frac{\partial}{\partial t} \Psi(\mathbf{r}, t) = \left(-\frac{\hbar^2}{2m} \nabla^2 + V(\mathbf{r}) + g \left| \Psi(\mathbf{r}, t) \right|^2 \right) \Psi(\mathbf{r}, t), \tag{1.1}$$

where $\Psi(\mathbf{r}, t)$ is the macroscopic wave function of the condensate and normalised to the number of bosons N in the condensate ($\int |\psi(r,t)|^2 d\mathbf{r} = N$), $V(\mathbf{r})$ is the external confining potential, and g is a coefficient that describes the effective interaction and relates to the s-wave scattering length a through $g = (4\pi\hbar^2 a/m)$ [4], (s-wave scattering is the isotropic low energy scattering when interaction potential decays sufficiently fast at infinity, and is on the order of the Borh radius (0.053 nm) [14]). The GP equation is a cubic NLS equation as the atom-atom interactions are represented by the cubic term $g|\Psi|^2\Psi$. It is widely used for the theoretical study of BEC [19].

In a BEC, the scattering length a (or nonlinear constant g) can take either positive or negative values and its sign and magnitude is of major importance, as it has a huge effect on the dynamics of Equation (1.1) [2]. A BEC with negative a is composed of atoms with attractive interactions and supports a kind of wave solution called a 'bright soliton', which is a localised nonlinear wave against a zero background. A BEC with positive a is repulsive and supports a different wave solution called a 'dark soliton'. A dark soliton is also a localised nonlinear wave, but it is termed 'dark' because its magnitude denotes a deficiency of the density with respect to a non-zero bulk value [19]. The scattering length depends on the atom species, but both the sign and magnitude are subject to change with Feshbach Resonance [5]. By tuning an external magnetic (or optical and electric) field in the vicinity of a Feshbach resonance, experimentalists are able to manipulate atomic collisions and change the sign and strength of atomic interactions [2]. A BEC under such manipulation is said to be collisionally inhomogeneous if different point in space experiences different scattering monitoring. In the context of this dissertation, one may think of collisional inhomogeneity as a spatial modulation of the scattering length.

Another essential experimental technique in studying BEC is control of the external potential. A variety of different potentials have been implemented in laboratories, including magnetic traps (MT), optical lattices (OL), optical superlattices (OSL), double-well traps, and superpositions of lattices or superlattices with magnetic traps [20]. Magnetic traps create a harmonic (parabolic) potential [3]. Optical lattices are implemented by the interference of two or multiple laser beams and are of periodic potentials. Optical superlattices are realised by the sequential creation of two optical lattices and provides a periodic or quasi-periodic potential that features two different periods [17]. The shape and time variation of the external potential can be tuned accurately and flexibly, which enables different nonlinear waves and have been demonstrated in both experimental and theoretical studies [2].

BECs support a variety of types of solutions, including plane waves [21], solitary waves, and in higher dimensions, vortices [13]. Moreover, the macroscopic wave function $|\Psi(\mathbf{r}, t)|$ (also called the condensate wave function) in the GP Equation (1.1) is normalised to the number of atoms, so its magnitude $|\Psi(\mathbf{r}, t)|^2$ represents atom density instead of probability. As a result, these solutions are observable macroscopically and are termed solitary matter-waves. In this dissertation, we focus on solitary matter-waves. In BECs the three most common types of solitary waves are bright solitons, dark solitons, and gap solitons. There is a wealth of theoretical work in studying the existence and stability of different solitary waves under various settings, among which the most comprehensive summary is given by Carretero-González et al. in the paper [2]. This paper is a great resource for relevant BEC background theory and mathematical techniques, from which we have adopted the basic concepts and methodology in our investigation.

This dissertation focuses on solitary waves in BECs in one-dimension in a magnetic trap and with spatially varying scattering length through Feshbach resonance. In the rest of the thesis, we will refer to it as a 'nonlinear lattice'. BECs with a nonlinear lattice have been studied theoretically in various papers. For instance, in [9] the authors studied 'long' solitary waves that span a large number of lattice periods with a general periodic nonlinear lattice and zero confining potential, using multiple-scale perturbation theory. In [6] and [22], the authors examine of 'short' solitary waves, the width of which is of similar magnitude to the lattice period in symmetric periodic nonlinear lattices with zero confining potential. In these papers, bright soliton and dark soliton solutions are identified, respectively, at the maximum and minimum within a lattice period.

Despite these theoretical predictions of phenomena in collisionally inhomogeneous BECs, so far no experimental implementations have been carried out. Our work specifically uses a model of the nonlinear lattice that is close to reality. It was proposed by an experimental physicist, Ian Spielman of University of Maryland and NIST, who confirmed in correspondence that such a model is experimentally feasible. In addition to the spatial modulation, it includes a temporal factor to simulate the dynamical of turning on a Feshbach resonance. We aim to examine the existence, stability, and dynamics of both bright and dark solitary waves using a spatially periodic nonlinearity introduced by Feshbach resonance. We will also inspect the response of the BEC to a sudden change or a gradual change of the atomic interactions. By providing a realistic picture, we hope that experimental physicists will check our results experimentally.

This thesis is organised as follows: In Chapter 2, we present the derivation of the GP equation from the many-body Hamiltonian describing the BEC and reduce the full 3D equation to a quasi-1D one with a highly anisotropic magnetic trap. We then study its ground-state properties and introduce the Thomas-Fermi approximation. We also discuss properties of the GP equation, emphasising its linear limit and nonlinear waves that bifurcate from the limit. In the last section, we introduce our model of the nonlinearity coefficient.

We give a detailed introduction to solitary waves in BECs in Chapter 3. We briefly explain solitary waves and their properties and then obtain closed-form solutions for bright and dark soliton solutions in BECs under the simplest setting, for which g is constant and the confining potential is zero. We also introduce a criterion for determining the linear stability of a soliton solution and derive the well-known Bogoliubov-de Gennes (BdG) equation. We have carried out numerical results, in which we have identified several soliton solutions using the stationary GP equation. We have studied its stability through BdG equation and examined its temporal evolution with the time-dependant GP equation to corroborate our stability analysis.

In Chapter 4, we present numerically obtained figures illustrating stability within a large range of parameters. We also present relevant theories of perturbed Hamiltonian systems and Hamiltonian flows in an attempt to explain some of the features that we have observed.

In Chapter 5, we examine the dynamical behaviour when the Feshbach resonance is turned on after stationary soliton solutions have already been built up. We investigate both fast and slow turning-on.

In Chapter 6, we conclude and discuss our results.

We discuss the numerical implementation in Appendix.

Chapter 2

Preliminaries

In this chapter, we introduce the fundamental equation in the theoretical study of BEC, the Gross-Pitaevskii (GP) equation, and the reduction to its quasi-1D equation. To examine the existence of nonlinear-wave solutions to the GP equation, we present the discrete spectrum of the linear part of the NLS operator, and then use Lyapunov-Schmit theory to establish nonlinear waves bifurcating from this linear limit under a small disturbance and with constant nonlinearity coefficient. We also introduce our basic setting for this dissertation: the model of the collisionally inhomogeneous BEC.

2.1 Quasi-1D Gross-Pitaevskii (GP) mean-field model

2.1.1 3D GP mean-field model

A BEC is a N-body Hamiltonian system composed of up to several million atoms [4], and a direct solution of the N-body problem is impossible. Instead, one introduces the GP mean-field model to study BECs theoretically. Starting from the fundamental N-body Hamiltonian system governed by Heisenberg equation, there are several ways to derive the mean field model. A rigorous derivation with a variational method can be found in [5]. Here we follow a much simpler but intuitive method from a review article of available mathematical methods in analysing nonlinear waves in BECs [2]. Taking into account the atom-atom interaction, the Hamiltonian of the BEC is written as

$$\hat{H} = \int_{\mathbb{R}^3} d\mathbf{r}\hat{\Psi}^\dagger(\mathbf{r},t)\hat{H}_0\hat{\Psi}(\mathbf{r},t) + \frac{1}{2}\int_{\mathbb{R}^3} d\mathbf{r}d\mathbf{r}'\hat{\Psi}^\dagger(\mathbf{r},t)\hat{\Psi}^\dagger(\mathbf{r}',t)V_I(\mathbf{r}-\mathbf{r}')\hat{\Psi}(\mathbf{r}',t)\hat{\Psi}(\mathbf{r},t), \tag{2.1}$$

where $\hat{\Psi}(\mathbf{r},t)$ ($\hat{\Psi}^\dagger(\mathbf{r},t)$) is the field operator creating(annihilating) a particle at the point $\mathbf{r}$, $\hat{H}_0 = -(h^2/2m)\nabla^2 + V(\mathbf{r})$ is the single-particle Hamiltonian, V is the external

potential to confine the BEC, and $V_I(\mathbf{r}-\mathbf{r}')$ is the two-body interaction potential. $\hat{\Psi}(\mathbf{r},t)$ and $\hat{\Psi}^\dagger(\mathbf{r},t)$ satisfy commutation relations [19]

$$\left[\hat{\Psi}(\mathbf{r},t),\hat{\Psi}^\dagger(\mathbf{r}',t)\right]=\delta(\mathbf{r}-\mathbf{r}'),\qquad \left[\hat{\Psi}(\mathbf{r},t),\hat{\Psi}(\mathbf{r}',t)\right]=0. \tag{2.2}$$

Substituting the Hamiltonian into Heisenberg equation $i\hbar\left(\partial\hat{\Psi}/\partial t\right)=[\hat{\Psi},\hat{H}]$, we have

$$i\hbar\frac{\partial}{\partial t}\hat{\Psi}(\mathbf{r},t)=\left(\hat{H}_0+\int_{\mathbb{R}^3}d\mathbf{r}'\hat{\Psi}^\dagger(\mathbf{r}',t)V_I(\mathbf{r}'-\mathbf{r})\hat{\Psi}(\mathbf{r}',t)\right)\hat{\Psi}(\mathbf{r},t). \tag{2.3}$$

The next step is to apply the Bogoliubov approximation, which states that to the lowest-order approximation and at very low temperature (considerably lower than the critical temperature T_c), one can replace the boson field operator $\hat{\Psi}(\mathbf{r},t)$ with a classical field operator $\Psi(\mathbf{r},t)$. $\Psi(\mathbf{r},t)$ is the macroscopic wave function of the condensate and is defined as the expectation value of the field operator ($\Psi(\mathbf{r},t)\equiv\langle\hat{\Psi}(\mathbf{r},t)\rangle$). [19]

We shall further simplify the interaction potential to a delta function, assuming the temperature is well below T_c and that the interaction is weak [2]:

$$V_I(\mathbf{r}-\mathbf{r}')=g\delta(\mathbf{r}-\mathbf{r}'), \tag{2.4}$$

where g is the effective interaction constant related to the s-wave scattering length a through $g=4\pi\hbar^2a/m$.

Adopting the delta function interaction potential and the macroscopic wave function approximation and utilising the commutation relations, we reach a compact so-called *mean-field* description of the system in terms of the 3D GP equation:

$$i\hbar\frac{\partial}{\partial t}\Psi(\mathbf{r},t)=\left(-\frac{\hbar^2}{2m}\nabla^2+V(\mathbf{r})+g\left|\Psi(\mathbf{r},t)\right|^2\right)\Psi(\mathbf{r},t). \tag{2.5}$$

where $V(\mathbf{r})$ is the external potential.

Compared to the ordinary Schrödinger equation, we now have an extra cubic term $g\left|\Psi(\mathbf{r},t)\right|^2\Psi(\mathbf{r},t)$ to describe the interaction between bosons. If $g=0$, the equation reduces to an ordinary Schrödinger equation. As will be discussed later, the magnitude of g determines the strength of the nonlinearity and the sign of g plays a huge role in determining the dynamics of the condensate.

We also note that with static external potentials [5], the above macroscopic wave function $\Psi(\mathbf{r},t)$ is normalised to the number of atoms and thus is interpreted as the particle density

$$N=\int_{\mathbb{R}^3}\left|\Psi(\mathbf{r},t)\right|^2d\mathbf{r}. \tag{2.6}$$

The Gross-Pitaevskii energy obtained from 2.5 is written as

$$E = \int_{\mathbb{R}^3} d\mathbf{r} \left(\frac{\hbar^2}{2m} |\nabla \Psi|^2 + V |\Psi|^2 + \frac{1}{2} g |\Psi|^4 \right). \tag{2.7}$$

By simplifying the complex N-body problem into an elegant NLS equation with a cubic nonlinearity term, the GP equation has become the most powerful instrument in the theoretical analysis of BEC.

2.1.2 Reduction to quasi-1D GP model

Consider a BEC in a magnetic trap, which is usually approximated as a harmonic potential:

$$V(\mathbf{r}) = \frac{m}{2} \left(\Omega_x^2 x^2 + \Omega_y^2 y^2 + \Omega_z^2 z^2 \right), \tag{2.8}$$

where Ω_x, Ω_y, and Ω_z are the trap frequencies along each direction. The characteristic oscillator length with the magnetic trap is defined as $l_i = \sqrt{\hbar/(m\Omega_i)}, i = x, y, z$, which sets the length scale for the spatial size of the condensate and is generally several microns [14]. Another important characteristic length scale of a BEC is the healing length $\xi = (8\pi\rho a)^{-1/2}$, where ρ is the BEC gas density and a is the scattering length. Here ξ is the distance over which atom-atom iteration balances with the kinetics [19]. ξ also represents the width scale of nonlinear excitations in BECs and is often several microns, the same scale of the characteristic oscillator length [2].

To consider a ground state under the harmonic potential, we write the condensate wave function as

$$\Psi(\mathbf{r}, t) = \psi_0(\mathbf{r}) e^{-i\mu t/\hbar}, \tag{2.9}$$

where ψ_0 is real and normalised to the number of atoms, and $\mu = \partial E/\partial N$ is the chemical potential of the system [5]. We then have

$$\left(-\frac{\hbar^2}{2m} \nabla^2 + V(\mathbf{r}) + g\psi_0^2(\mathbf{r}) \right) \psi_0(\mathbf{r}) = \mu \psi_0(\mathbf{r}). \tag{2.10}$$

In the case of $g = 0$, the system reduces to a Hamiltonian in parabolic potential, and the ground state is given by the Gaussian profile [5]:

$$\Psi_0(\mathbf{r}) = \sqrt{N} \left(\frac{m\Omega_{ho}}{\pi\hbar} \right)^{3/4} \exp\left(-\frac{m}{2\hbar} (\Omega_x x^2 + \Omega_y y^2 + \Omega_z z^2) \right), \tag{2.11}$$

where $\Omega_{ho} = \sqrt{\Omega_x \Omega_y \Omega_z}$ is the geometric mean of the confining frequencies.

For a repulsive BEC ($g > 0$), atoms are pushed towards the rims of the condensate and resulting in a spatial variation of the density, which is given by the Thomas-Fermi (TF) approximation [2]:

$$\rho(\mathbf{r}) = \begin{cases} g^{-1}[|\mu| - V(\mathbf{r})], & |\mu| > V(\mathbf{r}), \\ 0, & \text{otherwise.} \end{cases}$$

We are concerned with 1D nonlinear wave solutions, and shall only consider an anisotropic trap. Hence let $\Omega = \Omega_x = \Omega_y$ and define $\nu = \Omega_z/\Omega$, i.e

$$V(\mathbf{r}) = \frac{m\Omega^2}{2}\left(x^2 + y^2 + \nu z^2\right). \tag{2.12}$$

In the limit $\nu \ll 1$, the confinement is tight in the transverse direction and weaker in the longitudinal direction, as the transverse dimension of the BEC (on the scale of transverse harmonic length $l_r \equiv \sqrt{\hbar/(m\Omega)}$, where $r^2 = x^2 + y^2$) is much smaller than the longitudinal dimension, which is on the scale of longitudinal harmonic length $l_z \equiv \sqrt{\hbar/(m\Omega_z)}$. This generates a cigar-shaped BEC [5].

We separate the wave function into a longitudinal component and a transverse component:

$$\Psi(\mathbf{r}, t) = \psi(z, t)\Phi(r, t), \tag{2.13}$$

where $\Phi(r, t) = R(r)e^{-i\gamma t}$, and γ represents the chemical potential in the transverse direction. Substituting this into Equation (2.5), we see that $R(r)$ and γ should satisfy

$$-\frac{\hbar^2}{2m}\nabla_r^2 R - \frac{1}{2}m\Omega^2 r^2 R + \gamma R = 0, \tag{2.14}$$

where $\nabla_r^2 = \partial^2/\partial x^2 + \partial^2/\partial y^2$.

Suppose the transverse function stays in its ground state under the strong confinement; we can then solve for $R(r)$ to obtain $R(r) = \pi^{-\frac{1}{2}} l_r^{-1} \exp(-r^2/2l_r^2)$. Substituting this into Equation (2.13), multiplying by the complex conjugate of $R(r)$, and integrating with respect to r, we reach the 1D GP equation:

$$i\hbar\frac{\partial}{\partial t}\psi(z, t) = \left(-\frac{\hbar^2}{2m}\frac{\partial^2}{\partial z^2} + V_{1D}(z) + g_{1D}|\psi(z, t)|^2\right)\psi(z, t), \tag{2.15}$$

where the coefficients of the 1D equation are given by $g_{1D} = g/(2\pi l_r^2)$ and $V_{1D}(z) = (1/2)m\Omega_z^2 z^2$. For convenience, we will denote g_{1D} and $V_{1D}(z)$ as g and $V(z)$ in the rest of the thesis.

It is worth noting that this quasi-1D equation is obtained by averaging a 3D equation over the transverse plane. In contrast, a genuine 1D equation is derived

from a 1D setting. Also, similarly techniques can be applied to get the same quasi 1D approximation if the external potential is of a different form and get the same form (for instance, using $V(z) = V_0 \cos^2(kz)$ in case of an optical lattice). In the 1D BEC, the harmonic oscillator length is $l_{ho} = \sqrt{\hbar/(m\Omega_{h_0})}$, and the effective healing length becomes $\xi = \hbar/\sqrt{n_0 g_{1D} m}$ where n_0 is the reduced 1D density [2].

By nondimensionalising z, μ, and t with ξ, $g_{1D}n_0$, and ξ/c, where c is the speed of light, we arrive at the dimensionless 1D GP equation:

$$i\frac{\partial}{\partial t}\psi(z,t) = \left(-\frac{1}{2}\frac{\partial^2}{\partial z^2} + V(z) + g|\psi(z,t)|^2\right)\psi(z,t). \tag{2.16}$$

2.2 Analysis of GP operator in the linear limit

One of the main thrusts in theoretical studies of BECs is the investigation of the existence and stability of certain wave solutions. A wave solution needs to persist for a certain amount of time before experimentalists are able to observe it. There are two major techniques in studying the stability: one is examine bifurcations from the underlying linear Schrödinger problem and the other is to start from the nonlinear limit and examine the system as a perturbed Hamiltonian system [2]. In this section, we show how to examine the stability of wave solutions from the linear Schrödinger equation. To do this, we need to review the linear limit of the GP operator, first in the presence of a harmonic field, and then in the superposition of a harmonic field and a periodic field. After this, we will use Lyapunov-Schmidt (LS) theory to examine the nonlinear wave solutions bifurcating from the linear limit.

2.2.1 Spectrum of linear Schrödinger operator

Our interests in the project lie primarily in a single magnetic trap setting. However the analysis of linear operator of the setting is quite similar to the linear operator in the presence of both a harmonic trap and a periodic optical lattice. We thus present the result from [10]. In such a setting, the governing GP equation is written as

$$i\psi_t = -\frac{1}{2}\psi_{zz} - \psi + g\left|\psi\right|^2\psi + \left(\frac{1}{2}\Omega^2 z^2 + \epsilon p(z+\zeta)\right)\psi, \tag{2.17}$$

where $\frac{1}{2}\Omega^2 z^2$ is the magnetic field, and $\epsilon p(z+\zeta)$ is a periodic optical trap of small magnitude with period L and a displacement ζ relative to the magnetic trap.

By making the transformations,

$$\tilde{x} := \Omega^{1/2}x, \quad \tilde{\zeta} := \Omega^{1/2}\zeta, \quad \tilde{t} := \Omega t, \quad \tilde{\psi} = \Omega^{1/2}\psi, \tag{2.18}$$

and dropping hats, we get the dimensionless equation

$$i\psi_t = -\frac{1}{2}\psi_{zz} + g\left|\psi\right|^2\psi + \left[\frac{1}{2}z^2 + \frac{\epsilon}{\Omega}p\left(\frac{z+\zeta}{\Omega^{1/2}}\right)\right]\psi. \tag{2.19}$$

The underlying linear operator is

$$\mathcal{L} := -\frac{1}{2}\partial_z^2 + \frac{1}{2}z^2 + \frac{\epsilon}{\Omega}p\left(\frac{z+\zeta}{\Omega^{1/2}}\right). \tag{2.20}$$

It is known that $\mathcal{L}$ has a discrete spectrum with simple eigenvalues and associated eigenfunctions form a complete orthonormal basis [10]. Using perturbation theory it is shown in [10] that when $|\epsilon/\Omega| \ll 1$, the eigenvalues satisfy

$$\Pi_j = \frac{1}{2} + j + \Pi_j^\eta \eta + \mathcal{O}(\eta^2), \tag{2.21}$$

where

$$\Pi_j^\eta = \cos\left(\frac{2\zeta}{\Omega^{1/2}}\right)e^{-1/\Omega}\sum_{m=0}^{j}(-1)^m\frac{2^m}{m!}\begin{pmatrix} j \\ m \end{pmatrix}\Omega^{-m}, \qquad j \in \mathbb{N}\cup\{0\}; \tag{2.22}$$

In a simpler case when only the harmonic potential is considered, the underlying linear operator is just that of a single particle in a harmonic potential,

$$\mathcal{L} := -\frac{1}{2}\partial_z^2 + \frac{1}{2}z^2, \tag{2.23}$$

whose spectrum is well-known and has closed form expression [10]

$$\sigma(\mathcal{L}) = \left\{\Pi_j^0 : \Pi_j^0 := \frac{1}{2} + j, \qquad j \in \mathbb{N}\cup\{0\}\right\}, \tag{2.24}$$

with corresponding eigenfunctions

$$s_j(z) = c_j H_j(z)e^{-\frac{x^2}{2}}, \quad H_j(z) = (-1)^j e^{z^2}\frac{d^j}{dz^j}\left(e^{-z^2}\right), \quad c_j = \left(2^j j!\sqrt{\pi}\right)^{-\frac{1}{2}}, \tag{2.25}$$

where $H_j(z)$ are Hermite polynomials.

2.2.2 Nonlinear waves bifurcating from the linear limit

Now we include the cubic term in the GP equation and examine the stability of the nonlinear waves bifurcating from the linear standing waves using Lyapunov-Schmidt theory (see [7, 11] for detailed illustrations). The problem we are considering now becomes

$$\mathcal{L}\psi = g\psi^3, \tag{2.26}$$

and we note that so far we are only dealing with constant nonlinearity coefficient g.

Knowing that the linear operator $\mathcal{L}$ has a discrete eigenvalue spectrum, we consider a bifurcation at $\Pi = \Pi_n$, set $\Delta\Pi = \Pi - \Pi_n$, and with the bifurcating solution as $\Psi_n(z) = \epsilon\psi_n(z) + \mathcal{O}(\epsilon^2)$ for $0 < \epsilon \ll 1$. The so-called 'bifurcation function' is

$$b(\epsilon, \Delta\Pi) := -\epsilon\Pi - g\langle\psi_n^2, \psi_n^2\rangle\epsilon^3. \tag{2.27}$$

The bifurcating nonlinear waves are determined using zeros of the bifurcating function. To have a non-trivial solution, we need $g\Delta\Pi < 0$. So we can find nonlinear waves bifurcating from the reference states of linear standing waves as long as the relation $g\Delta\Pi < 0$ is satisfied.

2.3 Model of a Bose-Einstein condensate with spatially and temporally modulated nonlinearity

We mentioned in Chapter 1 that in this dissertation, we consider the case when g is modulated both spatially and temporally:

$$i\frac{\partial}{\partial t}\psi(z,t) = \left(-\frac{1}{2}\frac{\partial^2}{\partial z^2} + V(z) + g(z,t)|\psi(z,t)|^2\right)\psi(z,t) \tag{2.28}$$

We will first study the stationary solution in a nonlinear lattice, in which $g(z,t)$ is periodic in z. In this case, we are only concerned with the stable stage after turning on the Feshbach Resonance , and hence only consider a spatial variation $g = g(z)$. We then need to model the effect of the nonlinear lattice with a function depending on z, denoting as $\Delta g(z)$, and the nonlinearity coefficient in studying the steady state stationary solutions is

$$g(z) = g_0 + \Delta g(z), \tag{2.29}$$

where $g_0 = 1$ for repulsive BECs and $g_0 = -1$ for attractive BECs, and the spatially varying part of the nonlinear lattice can be either aligned and misaligned:

$$\Delta g(z) = \begin{cases} \pm\frac{V_1}{1+V_2\sin(kz+\pi/2)} & \text{aligned,} \\ \pm\frac{V_1}{1+V_2\sin(kz)} & \text{misaligned.} \end{cases} \tag{2.30}$$

where $+$ is for repulsive BECs and $-$ for attractive BECs, $V_1 \in [0,1]$ is the magnitude of the disturbance, $V_2 \in [0,1)$ modulates the shape of the lattice as it is approximately sinusoidal when $V_2 \ll 1$ and becomes spike-like as V_2 increases close to 1, and k denotes the periodicity of the lattice. We include the sign explicitly in order that

we can keep V_1 and V_2 positive in studying both bright solitons and dark solitons. Furthermore, we consider two different configurations of the spatial modulation: one is the minimum in a lattice period overlapping the bottom of harmonic potential (referred to as an aligned lattice), and the second is when there is a $\pi/2$ displacement between the two minima (referred to as a misaligned lattice). The model is the most simplified version to describe realistic nonlinear lattice in laboratory.

Previous studies of BECs in nonlinear lattice have concentrated on a pure spatial modulation. In this dissertation we consider the realistic situation of turning on of the Feshbach Resonance and introduce a temporal modulation $T(t)$. In examining the dynamics, we begin with a spatially uniform nonlinearity coefficient g_0, and study the temporal evolution of the system with the nonlinear lattice turned on. The nonlinearity coefficient is then:

$$g(z,t) = g_0 + \Delta g(z)T(t), \tag{2.31}$$

with temporal model $T(t)$ defined as

$$T(t) = \frac{1}{2}\left(1 + \tanh\left(\frac{t-t_0}{\tau}\right)\right), \tag{2.32}$$

where t_0 denotes the time when Feshbach resonance is turned on. If t_0 is set to a positive value, $T(t)$ is 0 initially and reaches 1 when t is large enough. The transition time is determined by τ. In this way, we model the nonlinearity coefficient changing from an initial value of g_0 to a final value of $g_0 + \Delta g(z)$, as $\Delta g_s(z)$ represents modulation introduced by the Feshbach resonance. A very small τ describes a fast turning on, and a large τ describes a gradual one. Both of them can be implemented experimentally.

The temporal model (2.32) and spatial model (2.30) are plotted in Figure 2.1. In panel a, black curves represent the aligned lattice and red curves shows the misaligned lattice. The displacement of the misaligned lattice from the origin (which is at the minimum of the harmonic potential) is easily identified. One can also see that the curve with $V_2 = 0.1$ has different shape from that with $V_2 = 0.9$, so V_2 is called the 'shape- tuning' parameter. Also note that with the same $V_1 = 0.1$, the solid black curve (with V_2 =0.9) has a much larger peak value than the dashed black curve (with V_2 =0.1). This occurs because when V_1 and V_2 is fixed, $\Delta g(z)$ oscillates between $\pm\frac{V_1}{1-V_2}$ and $\pm\frac{V_1}{1+V_2}$, so the peak value also depends on V_2. Panel (b) shows the temporal modulation, revealing a transition from 0 to 1. $\tau = 0.1$ gives almost immediate transition from 0 to 1, and $\tau = 10$ gives a much longer transition time.

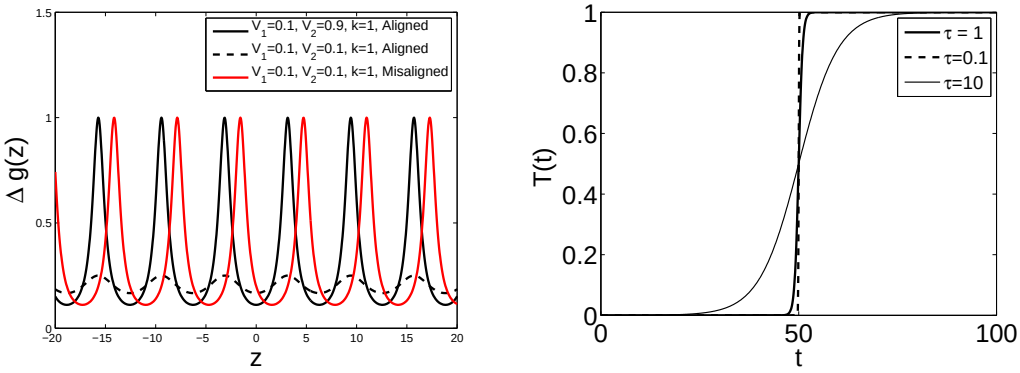

(a) Spatial modulation $\Delta g(z)$ (b) Temporal modulation $T(t)$

Figure 2.1: A model of spatially and temporally controlled $g(z,t)$.

Note that though it is possible to tune the scattering length from positive to negative using Feshbach resonance, in this dissertation we keep its sign unchanged. Otherwise the GP equation would be insufficient to describe the mean-field dynamics [19]. The spatial modulation $\Delta g(z)$ does not cross zero at all time that in this dissertation, and we use $V_1 \in [0,1]$, $V_2 \in [0,1)$ and $k \in [0,20]$. (In studying dark solitons in an misaligned lattice, k only ranges between 0 and 15).

Chapter 3

Solitary waves in BECs and their linear stability

3.1 Solitary waves: a brief introduction

In Chapter 1, we mentioned that BECs supports the existence of various soliton solutions. Strictly speaking, we should call them 'solitary waves', as soliton refers to the solution of a completely integrable system, while inclusion of either external potential or spatially varying nonlinear coefficient in our model makes it nonintegrable. However, the term 'soliton' is used widely for all localized wave solution in BECs [23], so in this thesis we use the terms 'soliton' and 'solitary waves' without distinction.

A solitary wave is one typical nonlinear wave that arises in systems governed by weakly nonlinear dispersive partial differential equations. In addition to NLS equations, there are also solitary solutions to the Korteweg-de Vries equation, the sine-Gordon equation, and other nonlinear partial differential equations. A soliton is a solitary wave that retains its shape when travelling at constant speed and can interact with other solitary waves and emerge from the collision without changing shape except for a phase shift. In this sense they behave like particles and is hence called 'solitons' [24].

Recalling our knowledge of waves, two key parameters in describing a wave include wave number and angular frequency. For a simple travelling plane wave, angular frequency does not depends on wave number, so components of different angular frequency travels at the same speed and the wave shape therefore does not change during propagation [16]. For a dispersive system, however, angular frequency is dependent on wave number, so the wave changes its shape as it travels. When nonlinear effects are taken into consideration, one can see intuitively that if nonlinear and dispersive

effects balance each other, the wave might propagate without shape deformation. Solitary wave arises when such a condition is satisfied [5].

3.2 Solitary waves in BECs

In Chapter 2 we claimed the existence of nonlinear wave solutions in a BEC. In this section, we first return to the 1D GP equation and identify soliton solutions. In searching for such localised waves, we suppose that we are considering a large enough region and set the boundary condition that both the wave function and its first derivative vanish at boundaries for bright soliton solutions. In finding a dark soliton solution, the boundary condition is that the wave function reaches a constant background value at boundaries while its first derivative vanishes [2].

3.2.1 Bright Solitons: attractive interaction

Here we show the basic steps in finding a closed-form soliton solution for attractive BECs ($g = -1$) in the absence of external potential [14]. Note that constant nonlinearity coefficient and zero external potential is a very strong requirement and closed-form solutions are not possible in most cases, so approaches like perturbative methods, variational methods, or other methods need to be adopted in finding analytical solutions in more complicated situations.

Starting from Equation (2.16), we search for a stationary wave solution $\psi(z,t) = u(z)e^{-i\mu t}$ where $u(z)$ is a real function and μ is the chemical potential of the system. Substituting into Equation (2.16) gives

$$\frac{1}{2}u_{zz} + \mu u + u^3 = 0. \tag{3.1}$$

Multiplying each term by u_z, integrating, given the boundary condition of $u = 0, u_z = 0$ as $z \to \pm\infty$, and rearranging gives,

$$\int \frac{du}{u\sqrt{2\mu + u^2}} = \int dz. \tag{3.2}$$

We let $\eta^2 = -2\mu > 0$, apply the transformation $u = \eta \operatorname{sech}\theta$, and utilize properties of hyperbolic functions to obtain

$$z = \frac{\theta - \theta_0}{\eta}, \tag{3.3}$$

where θ_0 is an arbitrary value, so the location of the soliton centre is free. By transforming back to the original variable, we obtain a standard bright soliton solution:

$$u(z) = \eta \text{sech}\left[\eta(z - z_0)\right] e^{-i\mu t}, \tag{3.4}$$

where η is the amplitude of the soliton, which is also inversely proportional to the soliton width. Chemical potential of bright soliton satisfies $\mu < 0$.

In the presence of a magnetic trap, bright soliton solution does not have a closed form. In Figure (3.1), we plot two bright soliton solutions with the magnetic trap $V = \frac{1}{4}z^2$ in a region $z \in [-100, 100]$ with $\mu = -10$ and $\mu = -100$, respectively. We can see that the wave function is normalised to the number of atoms. Observe that in the presence of the external potential, the one with larger μ (in magnitude) extends over a wider range than the one with smaller μ (in magnitude). In contrast, without the external trap, the one with $\mu = -10$ should be wider. Here the solution is obtained numerically. However, an approximate analytical expression can be sought with similar format to Equation (3.4) with variational method [2]. We will come back to this point in the next chapter.

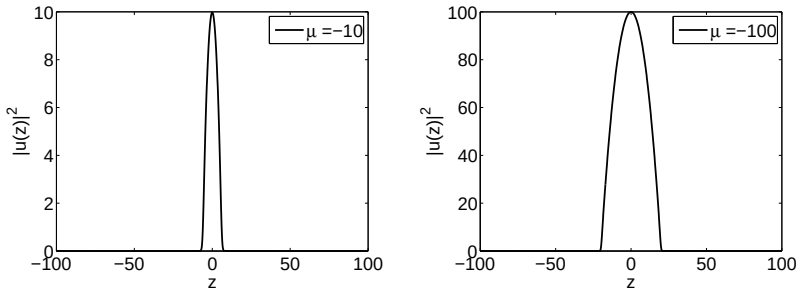

Figure 3.1: Stationary bright solitons in a BEC with a magnetic trap and $g = -1$.

3.2.2 Dark Solitons: repulsive interactions

Dark soliton solutions can arise in attractive BECs when the scattering length (and hence the nonlinearity coefficient) is positive. We seek a stationary solution $\phi(z, t) = u(z)e^{-i\mu t}$, for which u needs to satisfy

$$\frac{1}{2}u_{zz} + \mu u - u^3 = 0. \tag{3.5}$$

Using the same procedure as in Section 3.2.1, we find that the exact dark soliton solution in the absence of an external confining potential is

$$\psi(z, t) = \eta \tanh\left[\eta(z - z_0)\right] e^{-i\mu t}, \tag{3.6}$$

where $\mu = \eta^2$. Chemical potential of dark soliton satisfies $\mu > 0$.

Observing that the solution approaches η asymptotically as $z \to \pm\infty$, one can think of the solution as representing a deficit of condensate against a non-zero bulk value η.

In the presence of non-zero external potential, the situation is a bit different from that of a bright soliton in that when searching for a travelling wave solution, we need to find the travelling soliton on top of a static background. In other words, we seek the solution in the form of $\phi(z,t) = v(z)\exp(-i\mu t)u(z,t)$, where $v(z)$ is the background wave function and the new unknown function $u(z,t)$ represents the dark soliton [2].

In Figure 3.2 we plot two dark solitons with a magnetic trap $V(z) = \frac{1}{4}z^2$, with $\mu = 10$ and $\mu = 100$ respectively. Note that in the dissertation we compute soliton solutions in the region $z \in [-100, 100]$ but sometimes only present the figure in a smaller region.

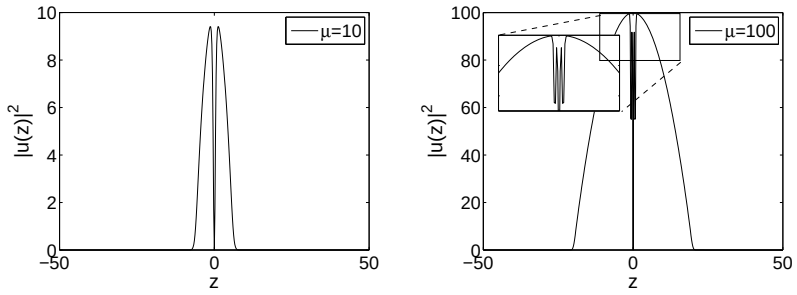

Figure 3.2: Stationary dark solitons in a BEC with a magnetic trap and $g = 1$.

3.3 Linear stability - BdG equation

A major task in studying nonlinear waves in BECs is to examine their stability. In this section, we introduce the Bogoliubov-de Gennes (BdG) equations as a means to determine the linear stability of a nonlinear wave solution.

To study the stability of small-amplitude excitations around a reference state, we linearise around the reference state and derive the BdG equation. First, we seek solutions of the forms

$$\psi(z,t) = \psi_0(z,t) + \delta\psi(z,t), \tag{3.7}$$

where $\delta\psi(z,t)$ is the small-amplitude excitation from the reference solution $\psi_0(z,t)$. By substituting $\psi(z,t)$ into (2.16), we obtain

$$i\frac{\partial}{\partial t}\left(\psi_0 + \delta\psi\right) = \left(-\frac{1}{2}\frac{\partial^2}{\partial z^2} + V(z) + g(z,t)|\psi_0 + \delta\psi|^2\right)\left(\psi_0 + \delta\psi\right). \tag{3.8}$$

Note that $|\psi(z,t)|^2 = [\psi_0(z,t) + \delta\psi(z,t)]\,[\psi_0^*(z,t) + \delta\psi^*(z,t)]$, we have at $\mathcal{O}(1)$ that

$$i\frac{\partial}{\partial t}\psi_0 = \left(-\frac{1}{2}\frac{\partial^2}{\partial z^2} + V(z) + g|\psi_0|^2\right)\psi_0. \tag{3.9}$$

At $\mathcal{O}(\delta\psi)$, we obtain

$$i\frac{\partial}{\partial t}\delta\psi = \left(-\frac{1}{2}\frac{\partial^2}{\partial z^2} + V(z) + 2g|\psi_0|^2\right)\delta\psi + g\psi_0^2\delta\psi^*. \tag{3.10}$$

Writing out the reference state as $\psi_0(z,t) = u(z)e^{-i\mu t}$, where $u(z)$ is the solution of the stationary 1D GP equation, we obtain

$$-\frac{1}{2}\frac{d^2}{dz^2}u(z) - \mu u(z) + V(z)u(z) + g|u(z)|^2u(z) = 0. \tag{3.11}$$

Perturb with $\delta\psi(z,t) = e^{-i\mu t}\sum_j[p_j(z)e^{-i\omega_j t} + q_j^*(z)e^{i\omega_j t}]$, where $p_j(z)$, $q_j(z)$ are small perturbations describing the condensate's linear response to the external perturbations that oscillate at frequencies $\pm\omega_j$. All p_j, q_j and ω_j are generally complex. We obtain the coupled equations for $p_j(z), q_j(z)$:

$$\omega_j p_j(z) = \left(-\frac{1}{2}\frac{d^2}{dz^2} + V(z) - \mu + 2gu^2(z)\right)p_j(z) + gu^2(z)q_j(z), \tag{3.12}$$

$$-\omega_j q_j(z) = \left(-\frac{1}{2}\frac{d^2}{dz^2} + V(z) - \mu + 2gu^2(z)\right)q_j(z) + gu^2(z)p_j(z). \tag{3.13}$$

Equations (3.12) and (3.13) together constitute the *Bogoliubov-de Gennes (BdG) equations*, which can also be derived using a purely quantum-mechanical approach [19]. Its solutions provide the frequency of elementary excitations of the system and a mens to determine the stability of the ground solution. If ω_j has positive imaginary part, then any small perturbation to the ground state solution grows exponentially. Otherwise, the perturbation will not grow. We will examine the stability numerically, using the reference state $u(z)$ obtained from Newtonian iterative solution of the stationary GP equation. We then use the Matlab command `eigs` to find its eigenvalues, which uses the Arnoldi method.

3.4 Stationary solitary waves

In this section we present numerical solutions to the stationary GP Equation (3.11). I obtained this with Newton iteration. For each solution, its stability eigenvalues are

calculated from BdG equations (3.12) and (3.13). As a reminder, here we look into spatially varying nonlinear coefficient in the form:

$$g(z) = g_0 + \Delta g(z), \qquad \Delta g(z) = \begin{cases} \pm\frac{V_1}{1+V_2\sin(kz+\pi/2)} & \text{aligned,} \\ \pm\frac{V_1}{1+V_2\sin(kz)} & \text{misaligned.} \end{cases} \tag{3.14}$$

In attractive BECs, $g_0 = -1$ and $\Delta g(z)$ takes the negative sign, while in repulsive BEC $g_0 = 1$ and $\Delta g(z)$ takes the positive sign.

3.4.1 Stationary bright solitons

We now discuss bright solitons in BECs In a magnetic trap and in both aligned and misaligned nonlinear lattice. Recall that by 'aligned', we mean that the minimum of the magnetic potential overlaps with a local minimum of the nonlinear periodic lattice.

In Figure 3.3 we show bright solitons in the presence of a nonlinear lattice with small magnitude and set parameters as $\mu = -100$, $V_1 = 0.1$, $V_2 = 0.5$, $k = 1$. The magnetic trap is $V(z) = (1/4)z^2$. The upper row is with an aligned lattice and lower row is with a misaligned lattice. The left panel shows atom density in position space, the middle panel shows atom density in momentum space, and the right panel shows the corresponding stability eigenvalues. The harmonic potential and the nonlinear lattice are also plotted in grey in the left panel. As can be seen, the peak value of $\Delta g(z)$ is smaller than 0.2 and appears sinusoidal. With such small disturbance, solitons in both situations are confined in the region where $|\mu| > V(z)$. In the aligned case, in which both the harmonic potential and nonlinearity coefficient $g(z)$ are symmetric, the obtained soliton is symmetric. In contrast, the soliton with the asymmetric $g(z,t)$ loses the symmetry. In momentum space the density displays a sharp spike around $k = 0$, suggesting a large number of atoms with the same speed. The stability eigenvalues are real in both cases, indicating that both of them are stable. We always show results in both position space and momentum space, as this is how BECs are observed and recorded in laboratories.

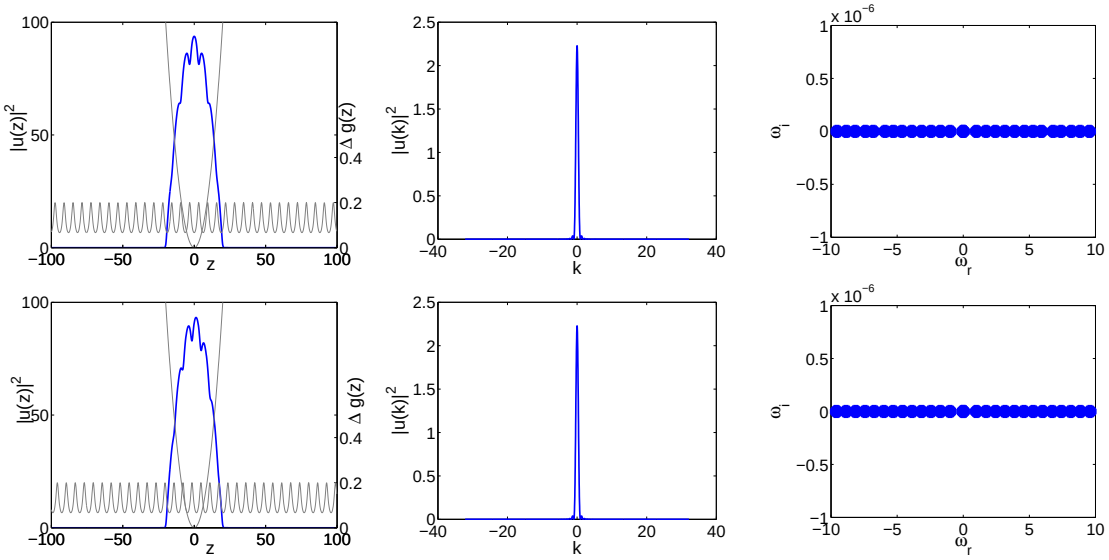

Figure 3.3: Stable bright solitons and their stability eigenvalues.

We have calculated stability eigenvalues of the bright solitons with parameters in the range $V_1 \in [0, 1]$, $V_2 \in [0, 0.95]$, $k \in [0, 20]$ and under a harmonic potential $V(z) = (1/4)z^2$. We calculated the stability eigenvalue with different V_1, V_2, k and have not found any eigenvalues with non-zero imaginary part. The maximum magnitude of its contribution to the nonlinearity coefficient is $\frac{V_1}{1-V_2}$, which reaches as large as 20 when $V_1 = 1$ and $V_2 = 0.95$. It seems that bright solitons in BECs with our model of the spatially modulated nonlinearity coefficient are always stable, despite the fact that the nonlinearity coefficient can be very large.

3.4.2 Stationary dark solitons

Now we present properties of dark solitons that we have found in both aligned and misaligned lattices. We examine the two lattices separately, as dark solitons behave differently in the two cases.

3.4.2.1 Stationary dark solitons in an aligned lattice

Compared to the bright solitons that we discussed in Section 3.4.1 that are always stable, dark solitons in both aligned and misaligned lattice can be either stable or unstable depending on the lattice parameters. Furthermore, in the aligned nonlinear lattice, unstable dark solitons have two different configuration of stability eigenvalues, one is with purely imaginary eigenvalues, and the other with a quadruplet of four eigenvalues with non-zero imaginary parts. We show the three different dark solitons in Figure 3.4. In sequence, we depict stable dark solitons (top row), unstable dark

solitons with pure imaginary stability eigenvalues (middle row), and unstable dark solitons with a quadruplet of complex stability eigenvalues (bottom row).

As in Figure 3.3, the right, middle, and left panels show the density in spatial space, density in momentum space, and stability eigenvalues, respectively. Parameters in the upper row are $V_1 = 0.2$, $V_2 = 0.5$, and $k = 1$; those in the middle row are $V_1 = 0.5$, $V_2 = 0.5$, and $k = 1$; and those in the lower row are $V_1 = 0.8$, $V_2 = 0.5$, $k = 2$. All three dark soliton solutions are with $\mu = 100$. Again the dark solitons are confined in the magnetic trap when chemical potential exceeds the trap potential, and all three dark solitons are symmetric. In both position space and momentum space, the wave density is zero at the origin, with two symmetric maxima at each side and close to the origin. In addition to the two largest maxima, there are several local maxima in both position space and momentum space. When k increases, the local maximum in momentum space is located at a larger value.

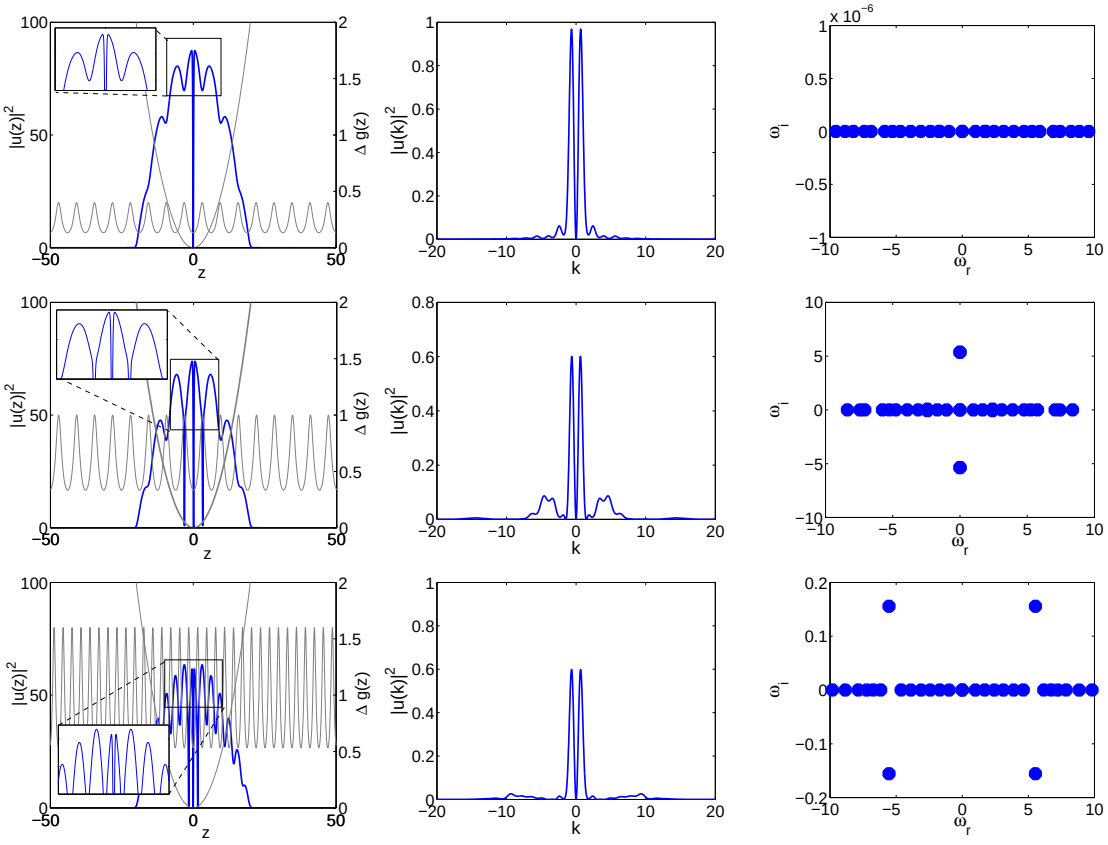

Figure 3.4: Dark solitons and their stability eigenvalues in an aligned lattice.

3.4.2.2 Stationary dark solitons in a misaligned lattice

In the presence of a misaligned nonlinear lattice, we find both stable and unstable dark solitons. In contrast to the aligned case in which unstable dark solitons can have either pure imaginary eigenvalues or a complex quadruplet of eigenvalues, in this case we have only identified unstable solitons with pure imaginary stability eigenvalues. This suggests a different bifurcation type from the aligned case, which we will discuss in the next chapter.

The organisation of Figure 3.5 is the same as in Figure 3.4 and Figure 3.3. The upper row depicts a stable dark soliton and the lower row depicts an unstable dark soliton. The Parameters for the stable dark soliton are $V_1 = 0.5$, $V_2 = 0.2$, and $k = 0.5$ and for the unstable dark soliton they are $V_1 = 0.1$, $V_2 = 0.5$, and $k_2 = 1$. In both the stable and unstable cases, the density always take non-zero values in either position space or momentum space, suggesting that we will not observe a complete 'darkness'. Furthermore, in both cases the maxima in position space are located at $x > 0$ and minimum at $x < 0$, but still very close to the origin. The origin is neither a maximum or a minimum, and the wave function is asymmetric. The density in momentum space is still symmetric, as Fourier transform of a real function is always even. However, in the upper row $k = 0$ is a maximum and in the lower row $k = 0$ is a minimum.

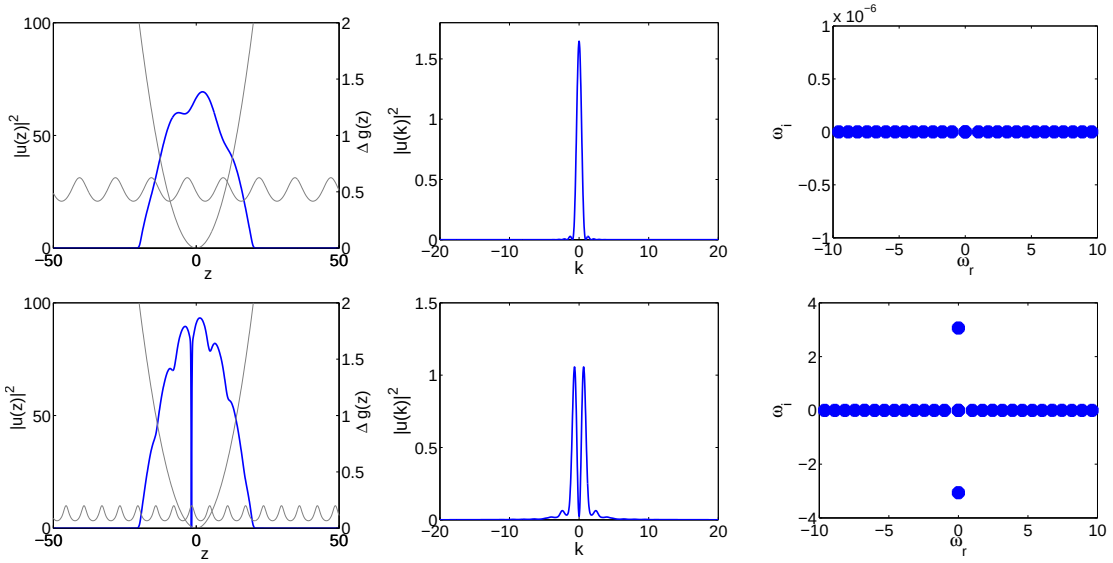

Figure 3.5: Dark solitons and their stability eigenvalues in a misaligned nonlinear lattice.

3.5 Temporal evolution of solitary waves with a static nonlinear lattice

In this section, we examine the temporal evolution of solitons in a static nonlinear lattice, so $g(z)$ is $g_0 + \Delta g(z)$, with $\Delta g(z)$ defined in Equation (2.30).

3.5.1 Temporal evolution of bright solitons

In this section we present the temporal evolution of a typical stable bright soliton in a BEC in an aligned lattice and choose the parameters as in top panel of Figure 3.3. We show the evolution of the bright soliton up to $t = 1000$ in Figure 3.6. The left upper panel shows the spatio-temporal evolution of $|u(z,t)^2|$ by a coloured contour plot, and the lower left panel shows the spatio-temporal evolution in momentum space. The right panels show the spatial profile of $|u(z,t)|^2$ at four values of time ($t = 0$, 200, 500, and 1000). This bright soliton is stable up to $t = 1000$.

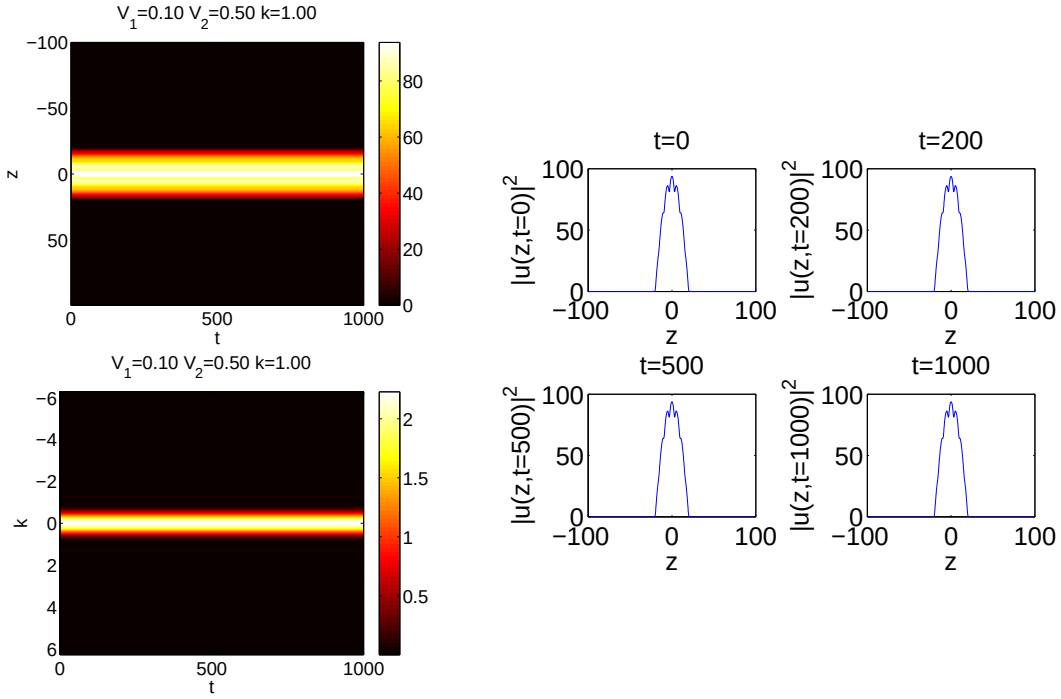

Figure 3.6: Temporal evolution of a stable bright soliton in an aligned lattice.

Though evolution of the stable soliton in a misaligned lattice is not presented, we have confirmed with computation that it is stable up to $t = 1000$.

3.5.2 Temporal evolution of dark solitons

3.5.2.1 Temporal evolution of dark solitons under an aligned lattice

In showing the temporal evolution of a stable dark soliton in an aligned lattice in Figure 3.7, we choose the same parameters as the upper row in Figure 3.4, except that the temporal evolution is plotted with $\mu = 10$. Before carrying out calculation with the new parameters, we have tested its stability eigenvalues and made sure they are all real. Organisation of Figure 3.7 is the same as in Figure 3.6. It is confirmed by the computation that this dark soliton is stable up to $t = 1000$ in both spatial space and momentum space.

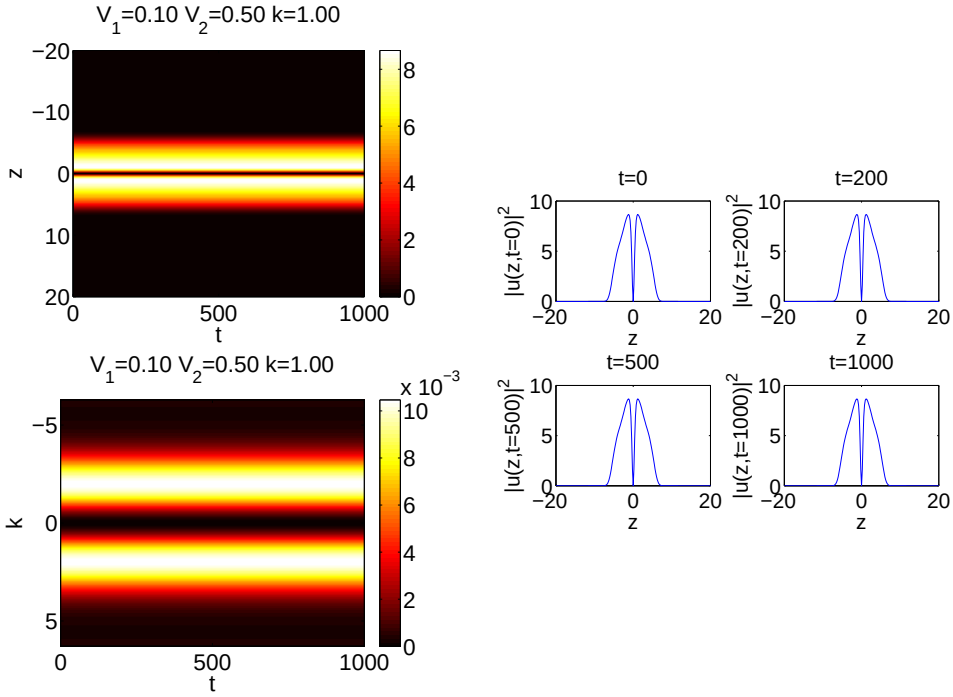

Figure 3.7: Evolution of a stable dark soliton in an aligned lattice.

In Figure 3.8, we present the time evolution of an unstable dark soliton in an aligned lattice with parameters $V_1 = 0.5$, $V_2 = 0.5$, $k = 1$ and $\mu = 10$. One can see from the spatio-temporal evolution in real space (upper left), evolution in Fourier space (upper right), and the density profiles at $t = 0$, 200, 500, and 1000 that the dark soliton breaks up around $t = 300$. The initially zero density at the centre of real space and momentum space is finally lost.

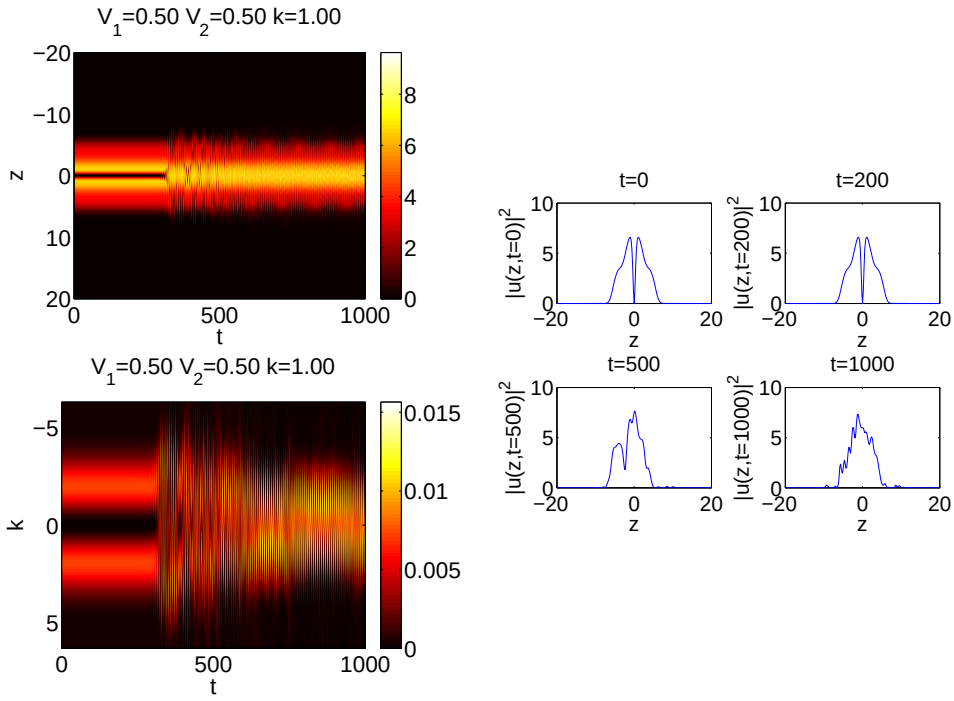

Figure 3.8: Temporal evolution of an unstable dark soliton in an aligned lattice.

3.5.2.2 Temporal evolution of dark solitons under a misaligned lattice

In Figure 3.9, parameters are $V_1 = 0.2$, $V_2 = 0.5$, $k = 2$ and $\mu = 10$. It is observed that instability happens at an early stage. We can see that after the lost of stability, the centre of dark soliton begins to oscillate at around $t = 25$, and disappears at around $t = 250$. We have confirmed in our calculations that the starting of instability is related to the magnitude of the largest imaginary eigenvalue. The larger the largest imaginary eigenvalue, the earlier stability is lost.

We have also confirmed that dark solitons in lower row of Figure 3.5 are dynamically stable through the evolution figure but do not present the figures here.

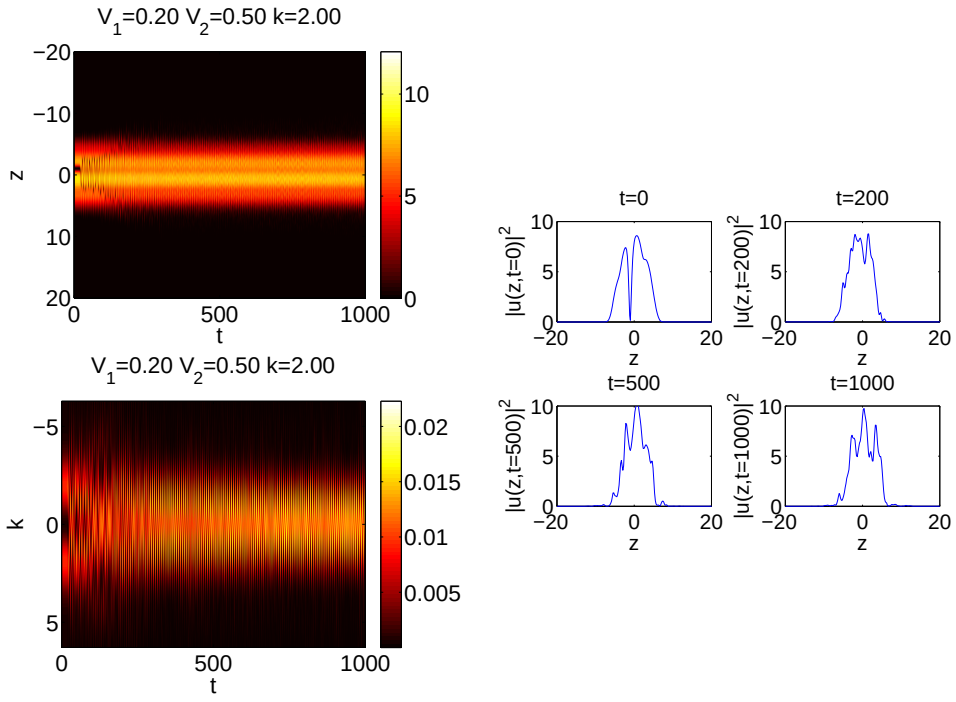

Figure 3.9: Evolution of an unstable dark soliton in a misaligned lattice.

Chapter 4

Stability of solitary waves

In Section 3.4, we found various stationary soliton solutions and examined their linear stability by computing eigenvalues through BdG equation. We also identified typical configurations of these eigenvalues. We found that bright solitons in both aligned and misaligned lattice are always stable within our parameter range. However, dark solitons could be either stable or unstable. While all unstable dark solitons with aligned nonlinear lattice are with imaginary stability eigenvalues, those with aligned nonlinear lattice are with both imaginary stability eigenvalues and quadruplet eigenvalues.

In this chapter, we aim to quantify the stability of different soliton solutions in a large range of parameter values through numerical simulation. However, corresponding theory to explain what we have observed is largely undeveloped, though in some cases there have been some perturbative analysis [9]. We present some analysis to corroborate our numerical results under appropriate conditions [2]. Meanwhile, we hope that our results will assist future development of the theory in this field.

4.1 Stability of a Hamiltonian flow

To better understand the several configurations of eigenvalues we have seen in Section 3.4, we present some basic theory in Hamiltonian system [15]. A Hamiltonian flow is written as

$$\dot{z} = J \cdot \mathrm{D}H_z \tag{4.1}$$

where $\dot{z}$ denotes the derivative of z with respect to time and $\mathrm{D}H_z$ is the Jacobian of H at z, and

$$J = \begin{pmatrix} 0 & I \\ -I & 0 \end{pmatrix} \tag{4.2}$$

so that $J^2 = -\mathrm{I}$.

The motion near the equilibrium z_0 is then

$$\delta\dot{z} = L\delta z, \tag{4.3}$$

where $\delta z = z - z_0$, $L = J \cdot \mathrm{D}^2 H$ is the linearisation, and $\mathrm{D}^2 H$ is the Hessian matrix of second derivatives. $\mathrm{D}^2 H$ is symmetric, so L is Hamiltonian.

If σ is an eigenvalue of L, then $-\sigma$, σ^*, $-\sigma^*$ are all eigenvalues of the system (though not necessarily distinct), as $J \cdot L$, L^*, $J \cdot L^*$ have eigenvalues $-\sigma$, σ^*, and $-\sigma^*$ respectively [15]. As a result, eigenvalues of a Hamiltonian flow always occur in pairs, including nonzero pure imaginary pairs, nonzero pure real pairs, nonzero complex quadruplets, and zero (of even multiplicity).

It is also stated in [15] that if all eigenvalues of an equilibrium z_0 of a Hamiltonian system with Hamiltonian H are pure imaginary and non-zero, and [15]$|I_\sigma$ is definite for each eigenvalue σ, then z_0 is linearly stable. When parameters vary, this equilibrium can lose spectral stability only by collision of eigenvalues for which $D^2 H|I_\sigma$ has opposite signature. That is, for such a such a system to be stable, every equilibrium must have eigenvalues that are either zero or pure imaginary.

Consider a Hamiltonian that depends smoothly on a parameter so that its eigenvalues vary continuously with the parameter. Imagine a pair of pure eigenvalues moving along the imaginary axis and meeting at the origin. If they pass each other and continue moving along the imaginary axes, the stability of the system is preserved; if the two collide into each other and generate a new eigenvalue quadruplet onto the complex plane, then the stability of the system is lost. This collision gives rise to a *Hamiltonian-Hopf bifurcation* [8].

Whether or not a Hamiltonian-Hopf bifurcation happens can be determined through the *Krein signature*. The Krein signature of a pure imaginary eigenvalue σ_n with corresponding eigenvector ζ_n is defined as:

$$\mathbf{K}_n := \mathrm{sign}(\zeta_k^T J L \zeta_k). \tag{4.4}$$

Krein's Theorem says that the when two eigenvalues with the same Krein signature meet, they remain on the imaginary axis. If two eigenvalues with opposite Krein signature meet, the collision might happen and the system would lose its stability.

Krein theorem is derived from ODE systems. However, in the book [15] it is stated that an infinite-dimensional Hamiltonian system can be decomposed into finite-dimensional blocks. The reduction explains that in our PDE system, only a small number of eigenvalues are controlling. While there are other eigenvalues exist, they

do not contribute. Hence the Krein's theory is applicable to our situation. We check our results in Section 3.4, where we have observed both pure real eigenvalues pair and complex quadruplet. Now we have calculated corresponding Krein signatures before and after different instability type happens, and we confirm that the results agree with Krein's theorem.

4.2 Effect of the nonlinear lattice on stability: computational results

In Chapter 3, our numerical results suggested that bright solitons in both aligned and misaligned nonlinear lattices are always stable, hence in this section we only discuss the stability of dark solitons.

4.2.1 Stability of solitons in an aligned nonlinear lattice

In the aligned nonlinear lattice, we have observed both pure real unstable eigenvalues and complex quadruplet eigenvalues. To examine the stability of dark solitons in an aligned nonlinear lattice, we record the maximum imaginary part of stability eigenvalues with different combinations of V_1, V_2, and k, where V_1 ranges from 0 to 1, V_2 ranges from 0 to 0.95, and k ranges from 0 to 15. Figure 4.1 shows the dependence of maximum imaginary eigenvalues on V_1 and V_2 for different k. We see that there is no monotonic dependence of the stability eigenvalues on the three parameters. In the medium k region (corresponding to figures 4.1(b)-4.1(f)), one can observe the dramatic change of the stability region with varying k. When k is small i.e. below 0.6, the maximum imaginary part of stability eigenvalues never exceeds the stability criterion 10^{-3} and the corresponding dark solitons are always stable. When k is relatively large i.e. $k > 7$, the dependence of maximum imaginary eigenvalues does not change dramatically. Figure 4.1(g) is plotted with $k = 7$ and shows that dark solitons are stable with smaller V_1 and V_2 but become unstable as one increases either V_1 or V_2. The trend of increased maximum imaginary part with increasing V_1 and V_2 suggests a stronger instability with larger Δg.

To see a general trend of eigenvalues with respect to k, in Figure 4.2 we fix V_1 and V_2 and plot the maximum imaginary values with k varying between 0 and 15. We plot each figure in upper panels using a fixed V_1, and we compare the maximum imaginary eigenvalue's dependence on k under different V_2. In the large k regime, one can observe larger stability eigenvalues with larger V_1 or V_2. When k is larger than 7, dark solitons tend to be unstable unless when V_2 is very small (see the $V_2 = 0.05$

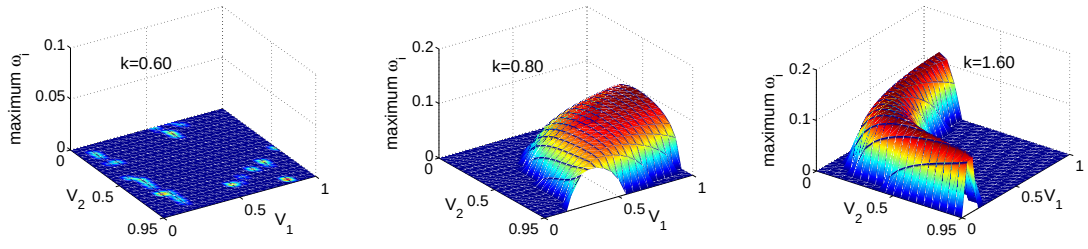

(a) $k = 0.6$ (b) $k = 0.8$ (c) $k = 1.6$

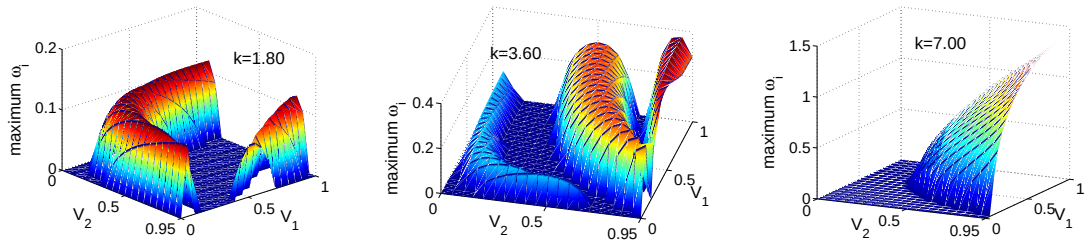

(d) $k = 1.8$ (e) $k = 3.6$ (f) $k = 7.0$

Figure 4.1: Maximum imaginary part of stability eigenvalues of dark solitons with aligned lattice.

curves in figures 4.3(a)-4.3(c)), or with a very small V_1 (0.05) and relatively small V_2 ($0.05-0.5$), as suggested in the $V_2 = 0.05$, 0.25, and 0.5 curves in Figure 4.2(a). Recall that k represents the lattice periodicity, V_1 represents the amplitude of the nonlinear lattice, and V_2 represents the tuning of the lattice shape, with small V_2 yielding a shape similar to a sinusoid and a V_2 close to unity yielding a periodic sequence of sharp spikes. This suggests that if an aligned nonlinear lattice with very small spatial periodicity is created experimentally, stable dark solitons can be observed only when the magnitude of the lattice is small or when the shape of lattice is approximately sinusoidal.

We plot the lower panels in Figure 4.2 with a fixed V_1, and we compare the maximum imaginary eigenvalue's dependence on k for different V_2. We find similar conclusions as in the top row of figures, except for two points. One is in figure 4.2(e) with $V_2 = 0.05$, corresponding to an approximately sinusoidal lattice, when dark solitons are stable with larger k but exhibit instability with smaller k when V_1 is above 0.25. This is one of few cases when dark solitons can stay stable for large k. The other is in figure 4.2(g), where $V_2 = 0.95$ gives a lattice with repeated shape spikes. In such a situation, dark solitons are unstable for large k even when the magnitude

V_1 is as small as 0.05. This reveals that dark solitons in an aligned nonlinear lattice featuring densely spaced sharp spikes (hence large k) are always unstable, regardless of the magnitude of the spikes.

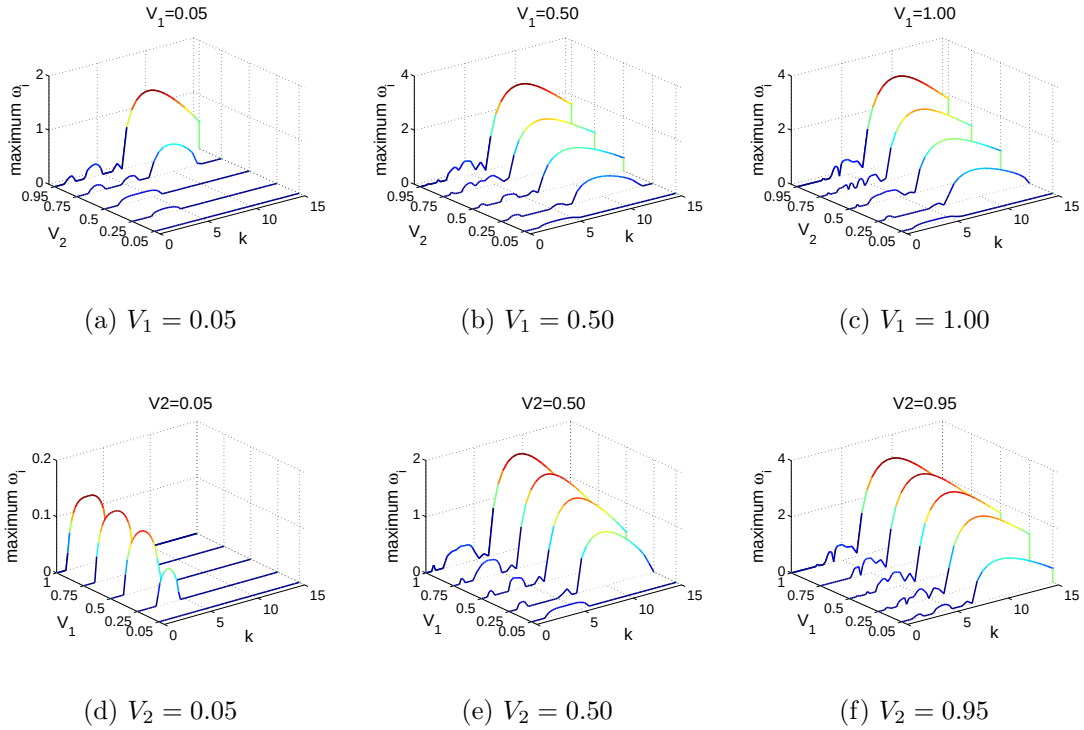

(a) $V_1 = 0.05$ (b) $V_1 = 0.50$ (c) $V_1 = 1.00$

(d) $V_2 = 0.05$ (e) $V_2 = 0.50$ (f) $V_2 = 0.95$

Figure 4.2: Maximum imaginary part of stability eigenvalues of dark solitons in aligned lattice with fixed V_1.

To further investigate how Figure 4.2(e) evolves into Figure 4.2(f), we present the dependence of eigenvalues on k with intermediate V_2 values in Figure 4.3, where V_2 takes 0.05, 0.15, and 0.35 each. In Figure 4.3(a), V_2 is the same as in Figure 4.2(e), but with more curves with different V_1 plotted. we confirm the instability in small k regime if V_1 is beyond a certain value, as we have discussed with 4.2(e). In Figure 4.3(a) this critical value for V_1 is determined to be 0.15. Dark solitons are always stable with $V_2 = 0.05$ and with varying k if V_1 is below or equal to this critical value. When V_2 increases, the stability with $V_2 < 0.15$ at smaller k region breaks up and instability at larger k develops, as we can spot in Figure 4.3(b) and 4.3(c).

Now our results explains how the stability is affected by varying k with different values of V_1 and V_2. However, as we have noticed from Figure 4.1 that in the smaller k regime, the situation is very complicated. We illustrate some of our findings in this medium k regime. To show this we plot Figure 4.4 using a constant $V_1 = 0.75$. It

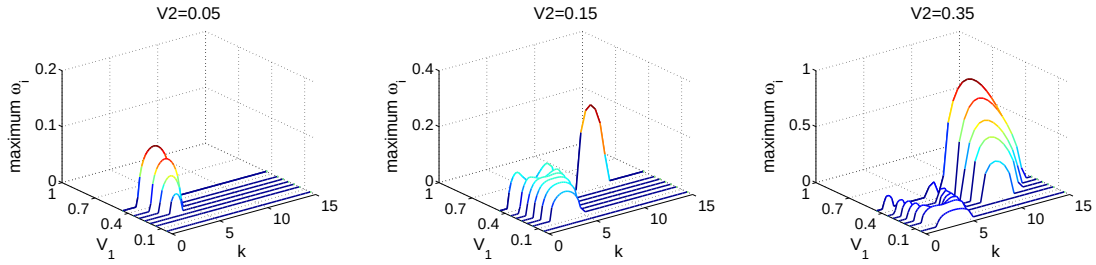

(a) $V_2 = 0.05$ (b) $V_2 = 0.15$ (c) $V_2 = 0.35$

Figure 4.3: Maximum imaginary part of stability eigenvalues of dark solitons in aligned lattice with small V_2.

shows the maximum imaginary stability eigenvalues' dependence on V_2 for different k. The upper panels show various configurations of the stable region (with respect to V_2) for specific k. Each figure of the lower panel is complementary to the one on top of it, with each k being 0.2 smaller than its top panel counterpart. The specific value of k is chosen that the stability region follows different patterns between the top panel figure and its lower panel counterpart. Hence one can see what happens with a relatively small change of k when bifurcation happens. In Figure 4.4(a) with $k = 0.8$, (and remember $V_1 = 0.75$), the positive maximum imaginary eigenvalues at $V_2 \in (0.1, 0.9)$ suggests an unstable region in this region. In comparison, Figure 4.4(e) shows that when k is 0.6 (and $V_1 = 0.75$), black solitons are always stable, irrespective of V_2. By comparing figure 4.4(a) and 4.4(b) we see that if V_2 is chosen a value in the unstable region of Figure4.4, corresponding dark solitons are initially unstable, but they would turn stable if k decreases from 0.8 to 0.6 (with $V_1 = 0.75$). We can interpret the rest figures of Figure 4.4 in the same way. Furthermore, if we term each unstable region with respect to V_2 as an instability 'window', the number and location of such windows are important in understanding the stability behaviour. By counting the number of instability windows in each figure, we see a clear change of the structure of stable regions. For instance, in the upper panels, from left to right, the number of instability windows is 1, 2, 3, and 2, respectively. In contrast, in the bottom panels, we observe 0, 1, 2, and 3 windows from left to right.

We observe similar 'window' structures with respect to V_1, when V_2 and k are fixed. We plot such windows with $V_2 = 0.75$ in Figure 4.5. The organisation is similar to Figure 4.4. Note that the location of the instability windows is as important in describing the stability as the number of windows. If we compare Figure 4.5(a) and 4.5(b), we would find that although we have one instability window in both figures,

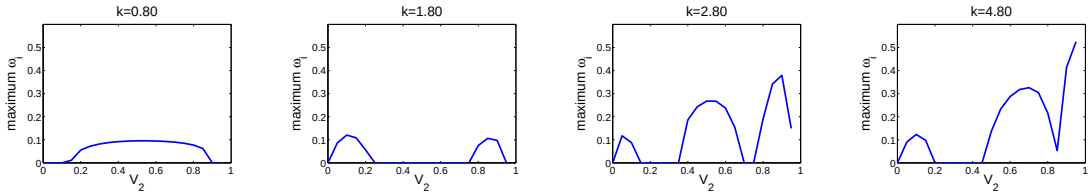

(a) $k = 0.8$ (b) $k = 1.8$ (c) $k = 2.8$ (d) $k = 4.8$

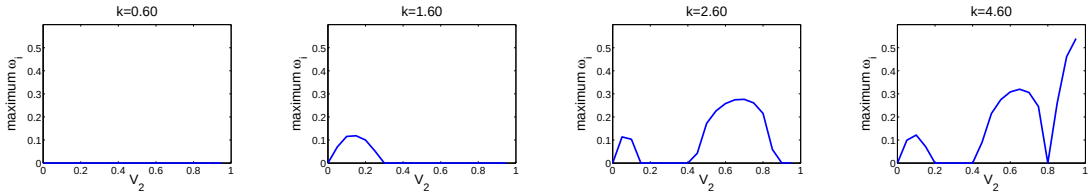

(e) $k = 0.6$ (f) $k = 1.6$ (g) $k = 2.6$ (h) $k = 4.6$

Figure 4.4: Maximum imaginary part of stability eigenvalues of dark solitons in an aligned lattice.

Figure 4.5(a) shows that dark solitons are stable with smaller V_1 and unstable with larger V_1, and Figure 4.5(b) shows an opposite trend, as dark solitons are unstable with smaller V_1 and stable with larger V_1. Another noticeable feature is that as k increases, firstly new windows are created as from Figure 4.5 (b) with $k = 1$ to Figure 4.5 (c) with $k = 1.8$. When k keeps growing to $k = 3.4$ as in Figure 4.5(d), a window disappears. If k continues growing, a new window is generated again, as in Figure 4.5 with $k = 3.8$. The creating and disappearing of the window structure with parameter changing is essential in understanding the bifurcation happening in the system, and will be further studied.

4.2.2 Stability of solitons under an misaligned nonlinear lattice

In the misaligned nonlinear lattice, the global picture of the stability dependence on the nonlinear lattice parameters is relatively straightforward. When V_1 and V_2 are fixed, the maximum imaginary part of the stability eigenvalues increases monotonically with k. That is, for every pair of V_1 and V_2, one just needs to find a cut-off value k_c. Dark solitons are stable when k is below k_c, and unstable when when k is larger than k_c.

We find this critical value by varying V_1 from 0 to 1 and V_2 from 0 to 0.95. In

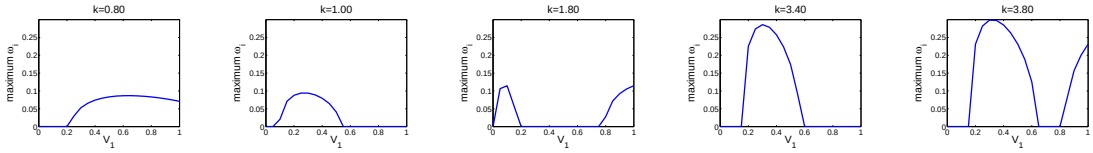

(a) $k = 0.8$ (b) $k = 1.0$ (c) $k = 1.8$ (d) $k = 3.4$ (e) $k = 3.8$

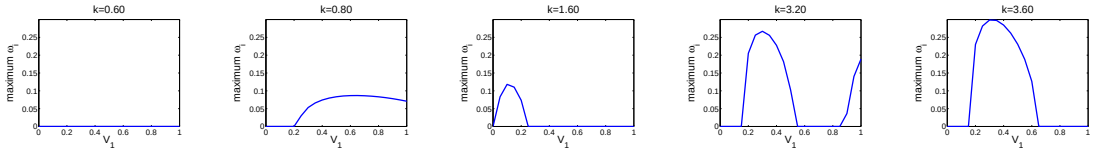

(f) $k = 0.6$ (g) $k = 0.8$ (h) $k = 1.6$ (i) $k = 3.2$ (j) $k = 3.6$

Figure 4.5: Maximum imaginary part of stability eigenvalues of dark solitons in an aligned lattice.

each searching, we start from $k = 0$ and increase k by increment of 0.2. If when k reaches 20 and no eigenvalue with non-zero imaginary part is found, the searching process is stopped and it is assumed that the system is always stable. In searching for the critical value, we set the criterion that a solution is unstable when its maximum imaginary eigenvalue (or the imaginary part of the eigenvalue) is larger than 10^{-3}. This value is determined empirically. Here we present the plot for the critical value k_c in Figure 4.6. The right panel is an overhead view, in which the region in dark brown represents when our search is stopped with $k = 20$, and hence denotes the stable region irrespective of k. We can see that when the nonlinear lattice magnitude is small or the lattice takes a nearby sinusoidal shape, dark solitons in the misaligned lattice are always stable even if the spatial periodicity of the lattice is very small. This trend is similar to what we have observed with dark solitons with an aligned lattice in Section 4.2.1.

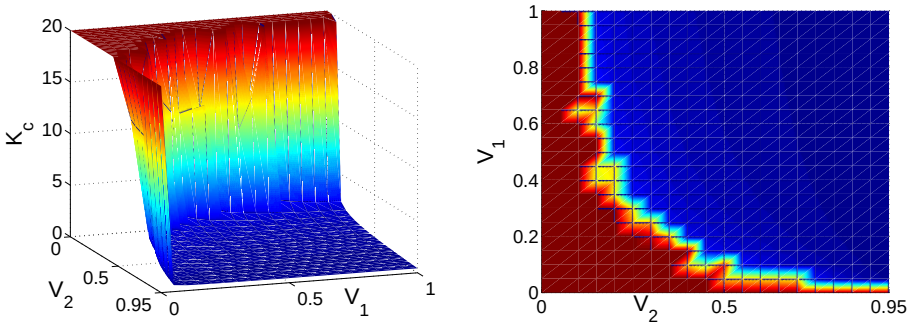

Figure 4.6: Cut-off values of k to determine stability with a misaligned lattice.

Chapter 5

Solitary waves in a temporally modulated nonlinear lattice

In this chapter, we show numerical computations of several solitary wave solutions. There is no theory in the literature that describes what happens when parameters describing the nonlinear lattice changes in a range. Instead we resort to numerical experiment as a first attempt to gain insight into the system.

5.1 Dynamics of travelling solitary waves

In this section we introduce a method called 'collective coordinates' to describe the movement of travelling solitary waves.

5.1.1 Bright Solitons

We obtained a closed-form solution for stationary solitary waves with zero external potential and constant nonlinearity coefficient. One can get travelling soliton solutions as [2]

$$u(z) = \eta \text{sech}\,[\eta(z - vt)]e^{i(kz-\beta t)}, \tag{5.1}$$

where the solitary wave number is k, frequency is β, the velocity v satisfies $v \equiv \frac{\partial \beta}{\partial k} = k$, and β satisfies the dispersion relation $\beta = \frac{1}{2}(k^2 - \eta^2)$ [2].

To consider the presence of an external field, we have an extra term of $V(z)u$ in left-hand side of Equation (3.1). We now assume that the solution can be written in the form

$$u(z) = \eta(t)\text{sech}\,[\eta(z - z_0(t))]e^{i(k(t)z-\alpha(t))} \tag{5.2}$$

where the soliton centre $z_0(t)$, phase $\alpha(t)$, and wavenumber $k(t)$ are unknown functions of t [2]. Suppose that the relations $k = \mathrm{d}z_0/\mathrm{d}t$ and $\beta(t) = (1/2)(k(t)^2 - \eta(t)^2)$ still hold. By substituting the ansatz into governing equations for the of atoms N and momentum P, and using the assumption that the external potential varies slowly one the scale of solitons, we can obtain the equation to describe the movement of bright soliton centre: (see [2] for a detailed derivation)

$$\frac{d^2 z_0}{dt^2} = -\frac{V}{z_0}, \tag{5.3}$$

In our setting with a magnetic trap, $V = \frac{1}{2}\Omega^2 z^2$,

$$\frac{d^2 z_0}{dt^2} = -\Omega^2 z_0. \tag{5.4}$$

So the centre of soliton oscillates like a single harmonic oscillator with frequency Ω, which we recall, represents the strength of the harmonic potential.

5.1.2 Dark Solitons

Travelling of dark solitary waves are more complicated than travelling bright solitons.

By adopting the same procedure in Section 5.1.1 and making the appropriate ansatz (see [2] for detailed derivation), we obtain a equation governing the motion of dark soliton centre as

$$\frac{d^2 z_0}{dt^2} = -\frac{1}{2}\frac{\partial V}{\partial z_0}. \tag{5.5}$$

As $V = \frac{1}{2}\Omega^2 z^2$, the oscillating frequency of the dark soliton is $1/\sqrt{2}$ of the confining strength [2].

5.2 Evolution of solitary waves in a dynamical nonlinear lattice

In Section 2.3, we introduced a model for the nonlinearity coefficient as the superposition of a spatial control and a temporal control in Equations (2.31) - (2.32). In this section we use the time dependent model for $g(z,t)$ and examine the temporal evolution of solitons in this situation. We only examine the aligned lattice in this section.

5.2.1 Bright solitons

In Figure 5.1, we present the temporal evolution of a bright soliton in an aligned lattice with $V_1 = 0.5$, $V_2 = 0.5$, $k = 0.5$. It is turned on quickly at $t = 50$ with $\tau = 0.1$. In Figure 5.1(a), we show its spatio-temporal evolution in both position space (left panel) and momentum space (right panel) up to $t = 200$. The middle panel is a magnified view with $t \in [45, 65]$ and $z \in [-40, 40]$. One can see that the system is no longer stable after $t = 50$, and in the position space we can observe an oscillation happening. In momentum space, atoms are initially centred at small k ($|k| < 1$), and at turning on the lattice, momentum of atoms is no longer concentrated.

Moreover, in the magnified view in the middle panel of figure 5.1(a), we can identify oscillations of bright centres and black centres, i.e. the travelling of both a high density of atoms and a zero density of atoms. This corresponds to travelling solitons we explained in Section 5.1.1 and Section 5.1.2. We follow the track of one travelling black soliton and record the time when it reaches its negative peak, crosses zero, and reaches its positive peak, (t_1, t_1, t_3 as labelled in the middle panel of figure 5.1(a)) and plot the spatial profile at each time t_1, t_1, t_3 in figure 5.1(c), from left to right. At t_1 and t_3, the travelling black soliton is at its peak values in space, and correspondingly the 'darkness' does not contribute to the density at origin, so the origin is a maximum. At t_2, the travelling black soliton happens to be crossing zero, and correspondingly the density at origin is a local minimum.

In Figure 5.1(b) the spatial profile at $t = 51$ (just after the turning on), $t = 100$, and $t = 200$ are plotted. By comparing these three profiles one can clearly spot oscillation in space.

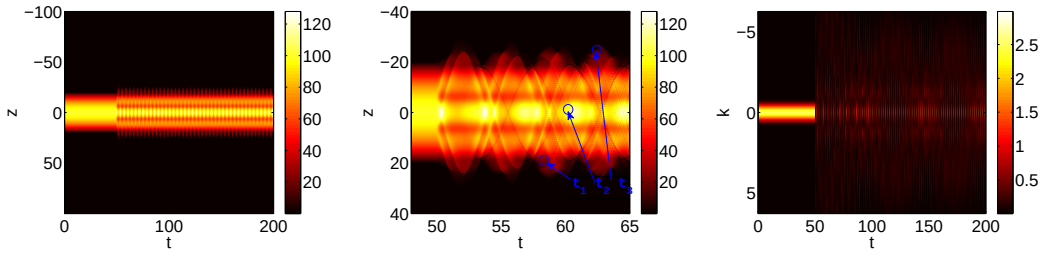

(a) Spatio-temporal plot in position space and momentum space.

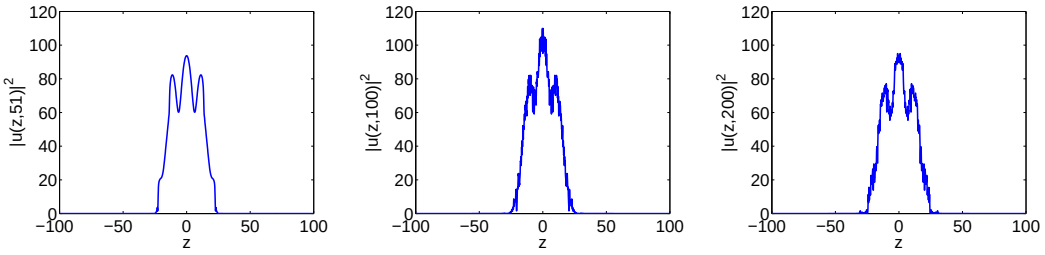

(b) Spatial profile at $t = 51$, $t = 100$, and $t = 200$.

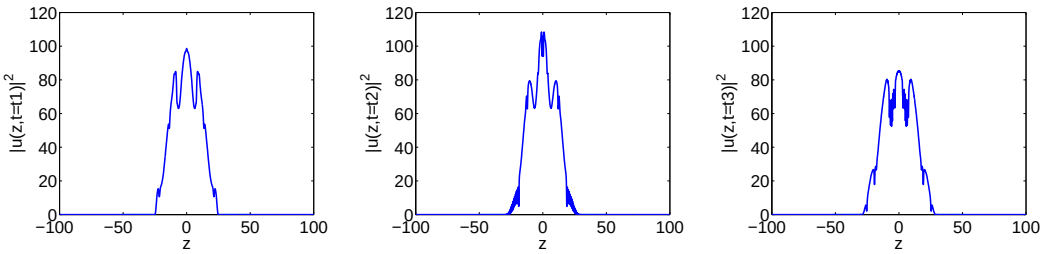

(c) Spatial profile when an emitted dark soliton travels from a negative peak to a positive peak.

Figure 5.1: Temporal evolution of a bright soliton in a nonlinear lattice that is turn on quickly.

Figure 5.1 shows the situation when a lattice is turn on quickly. To compare how the stability of the bright solitons in the nonlinear lattice is affected by the time needed to establish a steady-state lattice, we show a slow turning on in Figure 5.2(b) ($\tau = 10$) and a turning on with intermediate speed ($\tau = 1$) in Figure 5.2(a). In Figure 5.2(a), when it takes slightly longer time to establish the lattice than in Figure 5.1, we observe from the left panel and the right panel that solitons become unstable after $t = 50$. However, a magnified view in the middle panel suggests that there is no travelling dark solitons or bright solitons emitted.

A even slower turning on is shown in Figure 5.2(b), with $\tau = 10$. It can be seen that the transition is smooth that a steady state appears to be reached.

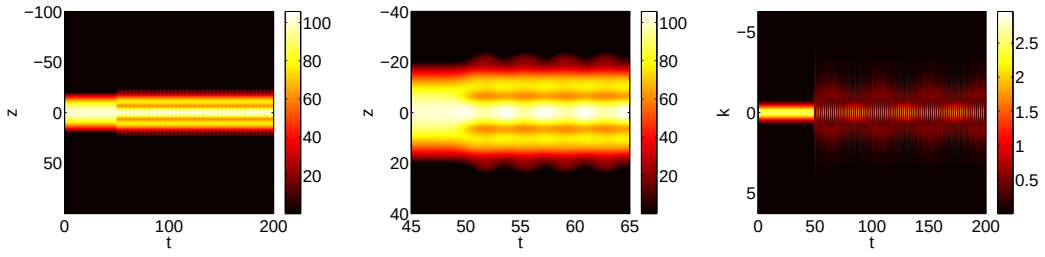

(a) $\tau = 1$

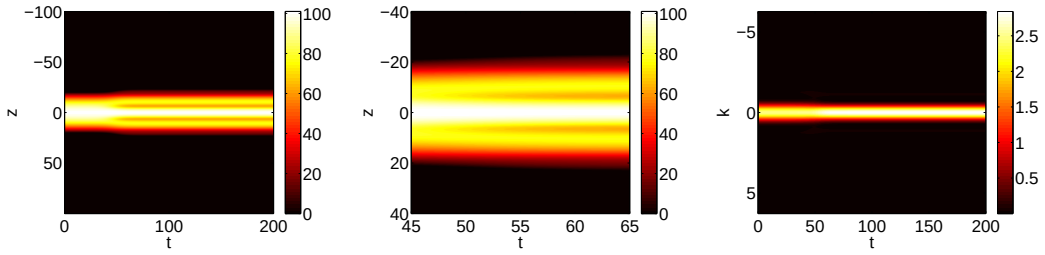

(b) $\tau = 10$

Figure 5.2: Evolution of a bright soliton in a lattice turned on in medium to slow speed.

We have also performed computations with larger k ($k = 1$ and 3). The trend is similar to what happens at $k = 0.5$. There are oscillations of a bright centre and dark centre when $\tau = 0.1$, and when $\tau = 10$ the transition is smooth and a steady state seems to be reached.

5.2.2 Dark solitons

In the dark soliton setting, we look at a more extreme case: a spike-like lattice with large magnitude and relatively small periodicity. Parameters for Figure 5.3 are $V_1 = 1$, $V_2 = 0.95$, $k = 3$, and $\mu = 10$. The organisation of the figures is the same as of Figure 5.2: the left panels correspond to the temporal evolution in position space and the right panels correspond to temporal evolution in momentum space, and the middle panels present evolution in position space with a magnified view. Figure 5.3(a)(b)(c) corresponds to $\tau = 0.1$, $\tau = 1$, and $\tau = 10$ respectively. It is shown similar trend as to Figure 5.2. For instance, in Figure 5.3(a), dark solitons become unstable after the lattice is turned on, and we can observe the emission of dark solitons and bright solitons in the middle panel. In Figure 5.3(b) with $\tau = 1$, dark solitons again become unstable after the nonlinear lattice is turned on, however no travelling solitons are

emitted. In Figure 5.3(c) when the turning on is slow, a smooth transition from the initial steady state to a final steady state is reached. The only difference might be in the rightmost panel in Figure 5.3(c), where we also spot a switch of the centre of density in momentum space.

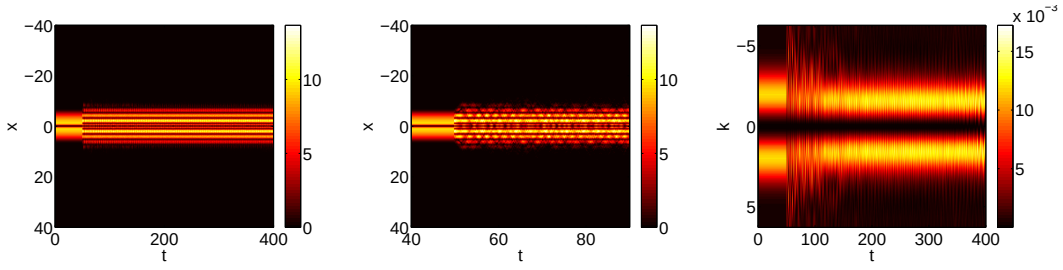

(a) $\tau = 0.1$

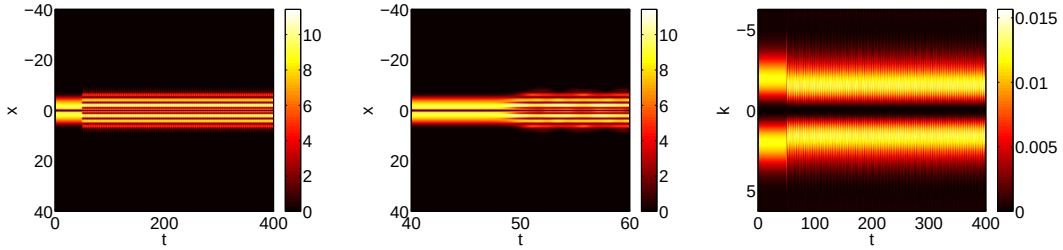

(b) $\tau = 1$

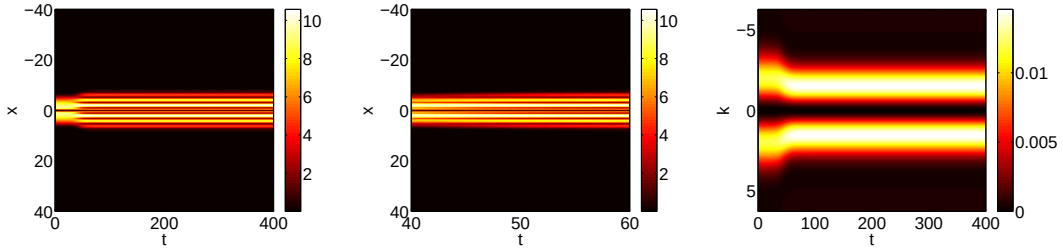

(c) $\tau = 10$

Figure 5.3: Temporal evolution of a dark soliton in a nonlinear lattice with three different speeds in turning on.

To summarise, in this Chapter we examine how the stability of bright solitons and dark solitons changes in a nonlinear lattice that is turned on with different speed. We have found that bright solitons and dark solitons tend to be stable if the lattice is turned on gradually, and tend to be unstable otherwise. If the lattice is turned on enough fast, we may also observe travelling bright solitons and travelling dark solitons.

Chapter 6

Conclusions

In this report, we examined the existence, stability, and dynamics of solitary waves in Bose-Einstein condensates in a nonlinear lattice and a magnetic trap using the GP equation. In previous studies of solitary waves in BECs in nonlinear lattices, the periodic nonlinear lattices were often modelled by sinusoidal functions, which did not describe the realistic situation accurately. In this work, we adopted a close to reality model of the nonlinear lattice as in 2.29 - 2.32. With this model, the shape and magnitude of the nonlinear lattice are both tunable, and in extreme cases the nonlinear lattice takes either an approximate sinusoidal shape or one with repeated sharp spikes. In addition to the spatial modulation, we also introduced a temporal modulation in order to study the dynamical response of solitary waves in BECs when the modulation is turned on. We have investigated solitons in BECs in both an aligned nonlinear lattice and a misaligned nonlinear lattice.

In the first part of the dissertation, we reviewed the basic theories of solitary waves in Bose-Einstein condensates with a periodic nonlinearity coefficient. This included an effort to present the derivation of the mean-field GP equation and its properties in Chapter 2, to present the BdG equations and explain the relevance to the stability of solitons in Chapter 3, to introduce the theory of perturbed Hamiltonian system and Hamiltonian flow to quantify the existence of stable soliton solutions with varying parameters in Chapter 4, and state the theory of collective coordinates to study dynamics of travelling solitons in Chapter 5.

These theories are essential for both analytical and numerical studies. In our computational experiments in Chapter 3, we first solved the stationary GP equation with Newton's method and found bright soliton solutions and dark soliton solutions. By computing their stability eigenvalues using the BdG equations, we identified stable bright solitons, stable dark solitons, and unstable dark solitons. No unstable bright solitons were found. Further examination revealed that in an aligned lattice, unstable

dark solitons in BECs could have either real eigenvalues or a quadruplet of four complex eigenvalues. In contrast, in a misaligned lattice, unstable dark solitons in BECs could only have real eigenvalues.

In Chapter 4 we continued with the stationary GP equation and computed the stability eigenvalues with varying parameters V_1, V_2, and k in the model for the nonlinear lattice Equations (2.29) - (2.32). We found that when k is large, i.e. the spatial periodicity of the nonlinear lattice is small, dark solitons tend to be unstable in both aligned and misaligned lattices. There is one exception: if the magnitude of the nonlinear lattice is small or if the shape of the lattice is approximately sinusoidal, dark solitons in both aligned and misaligned lattice can stay stable even if k is large. We also found that if an aligned nonlinear lattice is composed of repeated sharp spikes with very small spacing, dark solitons in the BEC in such lattice are always unstable even if the magnitude of the nonlinear lattice is quite small.

In Chapter 5, we studied the response of bright and dark solitons in BECs to the turning on of a nonlinear lattice, using the time-dependent GP equation. Numerical experiments suggest that a stable state can to be reached if the lattice is turned on slowly. In comparison, if the lattice is turned on abruptly, the system becomes unstable and both travelling bright and dark solitons can be emitted. Moreover, to observe the emission of solitons we need to turn on the lattice fast enough, as we showed that if the speed of turning on is in an intermediate region, the system becomes unstable but no solitons are emitted.

In this dissertation I have not examined the dynamics of bright and dark solitons in BECs in a misaligned lattice. This is left for future work. Another possibility of future work is to look into solitary waves in BECs with piecewise constant nonlinearity coefficient and a piecewise constant external potential. This setting was suggested by Professor P.G. Kevrekidis at the University of Massachusetts through correspondence, and experimentalists in UK are hoping to realise it. A similar setting with piece-wise constant nonlinearity and zero external potential has already been studied in [22].

Appendix A

Appendix

A.1 Numerical Solution stationary GP equation

Here we explain how we find the stationary solution to the 1D GP equation with a spatially varying nonilnearity. In the appendix we use a different set of notations.

The question we try to solve can be written as

$$i\phi_t = F(\phi), \tag{A.1}$$

where $F(\phi) = -\frac{1}{2}\phi_{xx} - \mu\phi + V(x)\phi + g(x)|\phi|^2\phi$. If we write $\phi(x) = u(x) + iv(x)$, then we transform the problem to obtain:

$$i(u_t + iv_t) = F(u + iv). \tag{A.2}$$

By expanding the form of F, we can get the equation set for u and v :

$$\begin{aligned} u_t &= F(v), \\ v_t &= -F(u), \end{aligned} \tag{A.3}$$

and we want to solve for

$$F(u) = F(v) = 0. \tag{A.4}$$

To discretise Equation (A.3), we choose the computational domain as $x \in [-100, 100]$ with a uniform spacing Δx. In vector form, it is written as $\mathbf{x} = \{x_1, x_2, \cdots, x_N\}$, where $N = 200/(\Delta x) + 1$.

We discretise u and v as $\mathbf{u} = \{u_1, u_2, \cdots, u_N\}$ and $\mathbf{v} = \{v_1, v_2, \cdots, v_N\}$, where $u_j \approx u(x_j), v_j \approx v(x_j)$ for $j = 1, 2, \cdots N$. If we define a new vector $\mathbf{w} = \{\mathbf{u}, \mathbf{v}\}$, then Equations (A.3) becomes:

$$F(\mathbf{w}) = 0, \tag{A.5}$$

which is solved through Newton Iteration.

Pseudo-code for Newton Iteration algorithm is:

Choose $\mathbf{w_0}$

Set $\mathbf{r_0}$ and j=1

while $\|r_j\| > \epsilon$ **do**

Calculate the Jacobian $J_{ij} = \frac{\partial F_i}{\partial w_j}$

Solve for $J\delta\mathbf{w}^k = -\mathbf{F}(\mathbf{w})$

Find $\mathbf{w}^{k+1} = \mathbf{w}^k + \delta\mathbf{w}^k$

Calculate r_{j+1}

$j = j + 1$

end while

By applying the specific form of our problem as $F(\phi) = -\frac{1}{2}\phi_{xx} - \mu\phi + \frac{\Omega^2 x^2}{4}\phi + g(x)|\phi|^2\phi$ and using the discretisation for $g(x)$ as $\mathbf{g} = \{g_1, \cdots, g_N\}$, we obtain the Jacobian as:

$$\begin{aligned}
J_{i,i} &= \frac{1}{h^2} - \mu + \frac{\Omega^2 x^2}{4} + g_i(3u_i^2 + v_i^2), \qquad i \le n, i \ne 1, n \\
J_{i,i-1} &= J_{i,i+1} = -\frac{1}{2h^2}, \\
J_{i,i} &= \frac{1}{h^2} - \mu + \frac{\Omega^2 x^2}{4} + g_i(u_i^2 + 3v_i^2), \qquad n+1 \le i \le 2n \\
J_{i,i-1} &= J_{i,i+1} = -\frac{1}{2h^2}, \\
J_{i,i+n} &= 2g_i u_i v_i, \qquad\qquad i \le n \\
J_{i,i+1} &= 2g_i u_i v_i, \qquad\qquad n+1 \le i \le 2n
\end{aligned} \tag{A.6}$$

By substitution of the specific Jacobian into the algorithm, we get the static solution with a proper initial guess. In searching for bright solitons, we use an initial guess $u_0 = \sqrt{\mu - \frac{\Omega x^2}{4}}$ in regions where $\mu > \frac{\Omega x^2}{4}$ and 0 otherwise, and initially $\mathbf{v}_0$ is set to be 0. In searching for dark solitons we use $u_0 = \tanh(x)\sqrt{\mu - \frac{\Omega x^2}{4}}$ in regions where $\mu > \frac{\Omega x^2}{4}$ and 0. Initial value for $\mathbf{v}_0$ is also zero. We choose $N = 2^{10}$ when $k < 3$ and N to 2^{12} with $k > 3$, as larger k implies faster oscillation, and one need more points in a period to approximate the shape of $g(x)$ accurately.

A.2 Time-dependent GP equation

We use fourth-stage Runga-kutta in solving the time dependent GP equation. We are given an initial value problem in the form:

$$\mathbf{y}' = \mathbf{f}(t, \mathbf{y}), \mathbf{y}(t_0) = \mathbf{y}_0 \tag{A.7}$$

The algorithm to solve this is:

$$\mathbf{y}_{n+1} = \mathbf{y}_n + \frac{1}{6}(\mathbf{k_1} + 2\mathbf{k_2} + 2\mathbf{k_3} + \mathbf{k_4}), \tag{A.8}$$

where

$$\mathbf{k_1} = h\mathbf{f}(t_n, \mathbf{y}_n); \tag{A.9}$$
$$\mathbf{k_2} = h\mathbf{f}(t_n + h/2, \mathbf{y}_n + \mathbf{k_1}/2); \tag{A.10}$$
$$\mathbf{k_3} = h\mathbf{f}(t_n + h/2, \mathbf{y}_n + \mathbf{k_2}/2); \tag{A.11}$$
$$\mathbf{k_2} = h\mathbf{f}(t_n + h, \mathbf{y}_n + \mathbf{k_3}), \tag{A.12}$$

where h is the time step.

In our situation, we only have to implement

$$\mathbf{w}_t = -i \times \left(-\frac{1}{2}\mathbf{w}_{xx} + \frac{\Omega^2}{4}x^2\mathbf{w} + g(x)|\mathbf{w})|^2\mathbf{w} \right)$$

A.3 Intrinsic frequency obtained from BdG equation

In section 3.3 we have the BdG Equations (3.12,BdG2), which we rewrite here:

$$\omega p(x) = \left(-\frac{1}{2}\frac{d^2}{dx^2} + V(x) - \mu + 2gu^2(x) \right) p(x) + gu^2(x)q(x),$$
$$-\omega q(x) = \left(-\frac{1}{2}\frac{d^2}{dx^2} + V(x) - \mu + 2gu^2(x) \right) q(x) + gu^2(x)p(x).$$

We take similar steps as solving the stationary GP equation, i.e discretise $p(x)$ and $q(x)$ as $\mathbf{p}$ and $\mathbf{q}$, combine $\mathbf{p}$ and $\mathbf{q}$ into a new vector $\mathbf{y}$, and convert the system into the form

$$A\mathbf{y} = \omega b \tag{A.13}$$

Then we can get the eigenvalue of A with Matlab function `eigs`.

Bibliography

[1] J. Butcher. Runge-Kutta methods. *Scholarpedia*, 2(9):3147, 2007.

[2] R. Carretero-González, D. J. Frantzeskakis, and P. G. Kevrekidis. Nonlinear waves in Bose-Einstein condensates: Physical relevance and mathematical techniques. *Nonlinearity*, 21:139–202, 2008.

[3] E. A. Cornell and C. E. Wieman. Bose-Einstein condensation in a dilute gas, the first 70 years and some recent experiments. *Reviews of Modern Physics*, 74:875–893, 2002.

[4] F. Dalfovo, S. Giorgini, L. P. Pitaevskii, and S. Stringari. Theory of Bose-Einstein condensation on trapped gases. *Reviews of Modern Physics*, 71:463–512, 1999.

[5] T. Dauxois and M. Peyrard. *Physics of Solitons*. Cambridge University Press, 2005.

[6] G. Fibich, Y. Sivan, and M. I. Weinstein. Bound states of nonlinear Schrödinger equations with a periodic nonlinear microsturcture. *Physica D*, 217:31–57, 2006.

[7] M. Golubitsky and D. Schaeffer. *Singularities and Groups in Bifurcation Theory, Vol. 1*. Springer-Verlag, 1985.

[8] J. Howard. Stability of Hamiltonian equilibria. *Scholarpedia*, 2007.

[9] G. Hwang, T. R. Akylas, and J. Yang. Solitary waves and their linear stability in nonlinear lattices. *Stud. Appl. Math*, to be published.

[10] T. Kapitula and P. G. Kevrekidis. Bose-Einstein condensates in the presence of a magnetic trap and optical lattice. *Chaos*, 15(3):37114, 2005.

[11] T. Kapitula, P. G. Kevrekidis, and B. Sandstede. Counting eigenvalues via the Krein signature in infinite-dimensional Hamiltonian systems. *Physica D*, 195(3-4):263–282, 2004.

[12] Todd Kapitula. Stability of waves in perturbed Hamiltonian systems. *Physica D*, 156:186–200, 2001.

[13] P. G. Kevrekidis and D. J. Frantzeskakis. Pattern forming dynamical instabilities of Bose-Einstein condensates: A short review. *Modern Physics Letters B*, 18:173–202, 2004.

[14] R. Kevrekidis, P. G.; Carretero-González. *The discrete nonlinear Schrödinger equation [electronic resource] : mathematical analysis, numerical computations and physical perspectives*. Springer, 2009.

[15] R. S. Mackay and J. D. Meiss. *Hamiltonian Dynamical Systems*. Adam Hilger, 1987.

[16] I.G. Main. *Vibrations and Waves in Physics*. Cambridge University Press, 1993.

[17] S. Peil, J. V. Porto, B. Laburthe Tolra, J. M. Obrecht, B. E. King, M. Subbotin, S. L. Rolston, and W. D. Phillips. Patterned loading of a Bose-Einstein condensate into an optical lattice. *Physical Review A*, 67:051603, 2003.

[18] C. J. Pethick and H. Smith. *Bose-Einstein condensation in dilutes gases*. Cambridge University Press, 2001.

[19] L. Pitaevskii and S. Stringari. *Bose-Einstein condensation*. Oxford: Clarendon Press, 2003.

[20] M. A. Porter and P. G. Kevrekidis. Bose-Einstein condensates in superlattices. *SIAM Journal on Applied Dynamical Systems*, 4:783–807, 2005.

[21] M. A. Porter, P. G. Kevrekidis, B. A. Malomed, and D. J. Frantzeskakis. Modulated amplitude waves in collisionally inhomogeneous Bose-Einstein condensates. *Physica D*, 229:104–115, 2007.

[22] A. S. Rodrigues, P. G. Kevrekidis, M. A. Porter, D. J. Frantzeskakis, P. Schmelcher, and A. R. Bishop. Matter-wave solitons with a periodic, piecewise-constant scattering length. *Physical Review A*, 78:013611, 2008.

[23] H. Sakaguchi and B. A. Malomed. Matter-wave solitons in nonlinear optical lattices. *Physical Review E*, 72:046610, 2005.

[24] N. J. Zabusky and M. A. Porter. Soliton. *Scholarpedia*, 5(8):2068, 2010.